# ORIGINAL RESEARCH

# Deciphering Brain Metastasis Stem Cell Properties From Colorectal Cancer Highlights Specific Stemness Signature and Shared Molecular Features

Amandine Desette,[1,2] Pierre-Olivier Guichet,[1,2] Sheik Emambux,[1,3] Konstantin Masliantsev,[1,2] Ulrich Cortes,[1,2] Birama Ndiaye,[1,2] Serge Milin,[1,4] Simon George,[5] Mathieu Faigner,[3] Julie Tisserand,[6] Afsaneh Gaillard,[7] Sébastien Brot,[7] Michel Wager,[1,8] David Tougeron,[1,9] and Lucie Karayan-Tapon[1,2]

[1]Université de Poitiers, CHU Poitiers, ProDiCeT, UR 24144, Poitiers, France; [2]Laboratoire de Cancérologie Biologique, CHU de Poitiers, Poitiers, France; [3]Service d'oncologie médicale, CHU de Poitiers, Poitiers, France; [4]Service d'Anatomie et de Cytologie Pathologiques, CHU de Poitiers, Poitiers, France; [5]MGX-Montpellier GenomiX, Université de Montpellier, CNRS, INSERM, Montpellier, France; [6]Pôle gériatrique, CHU de Poitiers, Poitiers, France; [7]Université de Poitiers, CHU de Poitiers, INSERM, LNEC, Poitiers, France; [8]Service de Neurochirurgie, CHU de Poitiers, Poitiers, France; and [9]Service d'hépato-gastro-entérologie, CHU de Poitiers, Poitiers, France

## SUMMARY

For the first time, stem cells of brain metastasis of colorectal cancer have been isolated and characterized at cellular and molecular levels in vitro, in vivo, and in silico.

**BACKGROUND & AIMS:** Brain metastases (BMs) from colorectal cancer (CRC) are associated with significant morbidity and mortality, with chemoresistance and short overall survival. Migrating cancer stem cells with the ability to initiate BM have been described in breast and lung cancers. In this study, we describe the identification and characterization of cancer stem cells in BM from CRC.

**METHODS:** Four brain metastasis stem cell lines from patients with colorectal cancer (BM-SC-CRC1 to BM-SC-CRC4) were obtained by mechanical dissociation of patient's tumors and selection of cancer stem cells by appropriate culture conditions. BM-SC-CRCs were characterized in vitro by clonogenic and limiting-dilution assays, as well as immunofluorescence and Western blot analyses. In ovo, a chicken chorioallantoic membrane (CAM) model and in vivo, xenograft experiments using BALB/c-nude mice were realized. Finally, a whole exome and RNA sequencing analyses were performed.

**RESULTS:** BM-SC-CRC formed metaspheres and contained tumor-initiating cells with self-renewal properties. They expressed stem cell surface markers (CD44v6, CD44, and EpCAM) in serum-free medium and CRC markers (CK19, CK20 and CDX-2) in fetal bovine serum-enriched medium. The CAM model demonstrated their invasive and migratory capabilities. Moreover, mice intracranial xenotransplantation of BM-SC-CRCs adequately recapitulated the original patient BM phenotype. Finally, transcriptomic and genomic approaches showed a significant enrichment of invasiveness and specific stemness signatures and highlighted KMT2C as a potential candidate gene to potentially identify high-risk CRC patients.

**CONCLUSIONS:** This original study represents the first step in CRC BM initiation and progression comprehension, and further investigation could open the way to new therapeutics avenues to improve patient prognosis. *(Cell Mol Gastroenterol Hepatol 2023;16:757–782; https://doi.org/10.1016/j.jcmgh.2023.07.008)*

*Keywords:* Cancer Stem Cells; Colorectal Cancer; Brain Metastases; Stemness Signature.

**B**rain metastases (BMs) are the most common intracranial tumors, with various frequencies depending on the primary tumor site.[1] BMs are associated with significant morbidity and mortality, with a median overall survival ranging from 10 months in breast cancer to 6 months in lung cancer and 5 months in colorectal cancer (CRC).[2,3] Treatment options are often multimodal, including surgery, stereotactic radiosurgery, whole brain radiotherapy, systemic treatments, and/or best supportive care, mostly depending on the number of metastatic lesions, BM size and location, patient's prognosis, and performance status.

The incidence of CRC BMs varies from 0.1% to 11.5% but appears to be increasing, largely because of improved treatment and prognosis of metastatic CRC (mCRC) patients with no prolonged overall survival of more than 30 months.[4,5] The presence of *RAS* mutations and lung metastases appears to be associated with the development of BMs

in CRC.[6] The mechanisms that lead tumor cells from solid tumors to preferentially spread to the brain are still poorly understood. Genetic signatures have been described as possibly being associated with the development of BMs; in half of the cases, although the tumor cells of BM possess the mutations of the primary tumor, they will accumulate secondary mutations of their own, thus promoting their dissemination.[7] Understanding the biology of BM from solid tumors is an urgent need to identify predictive factors of BM and potential druggable molecular pathways. There is therefore a need for an appropriate experimental model to study BM cells from solid tumors such as CRC.

There is growing evidence suggesting the implication of a subpopulation of cancer cells sharing stem-like properties, known as stem-like cells, tumor-initiating cells, or cancer stem cells (CSC), that are responsible for tumor initiation, maintenance, and progression.[8] Several studies have confirmed that CSCs are responsible for resistance to treatment and disease recurrence in primary solid tumors.[9–11] Moreover, the CSCs are thought to represent approximately 1% of the whole cancer cell population,[12,13] and interestingly, cells surviving to conventional cytotoxic treatment are enriched in cells with tumor-initiating and mesenchymal properties.[14] CRC cells expressing the CD133 surface marker were first identified as CSCs by Ricci-Vittani et al[13] and O'Brien et al[15] in the primary tumor site and secondary metastatic sites such as the liver and the peritoneum. Other markers such as aldehyde dehydrogenase 1 (ALDH1) activity, leucine-rich repeat-containing G protein-coupled receptor 5 (Lgr5), CD44, and epithelial cell adhesion molecule (EpCAM) were described as CRC-CSC markers as well.[16–18] In addition, CSCs expressing CD26 in primary CRC have been considered as CSCs with liver-metastatic potential.[19] CD44v6, another CSC marker, was also described to be associated with the metastatic potential because the expression of CD44v6 seems to be a prerequisite for the generation of

metastatic lesions.[20] Interestingly, circulating tumor cells (CTC) from blood of advanced mCRC patients were also described as bearing all the functional characteristics of CSC.[21] Furthermore, in a genetically engineered organoid model of intestinal tumorigenesis, selective ablation of Lgr5+ CSCs substantially restricted tumor progression.[22]

The presence of metastatic CSCs in BM has only been described very recently and for the first time in lung cancer and later in triple negative breast cancers.[23,24] Although some models have been developed for liver metastasis from CRC, to our knowledge, there are no data in the literature regarding the identification of metastatic CSCs in BM from CRC.

The aim of our study was to identify and characterize cells with stem-like cells properties in BM from CRC to identify potentially druggable molecular pathways in these particular cancer cell subpopulations.

## Results

### Colorectal Cancer–Derived Brain Metastases Cells Form Metaspheres Containing Tumor-Initiating Cells

Metastatic brain tumor samples were collected from 4 patients whose characteristics are summarized in Table 1. Cells were cultured in Dulbecco modified Eagle medium (DMEM)/F12 medium enriched with basic fibroblast growth factor (bFGF) and epidermal growth factor (EGF).

In these conditions cells have grown as spheres and formed metaspheres (Figure 1A). After dissociation and new culture, we observed formation of secondary and tertiary metaspheres. The secondary and tertiary sphere formation is considered as a hallmark of the stem cell property of self-renewal.[25] Thus, we were able to establish 4 BM stem-like cell lines derived from 4 CRC patients with resected BM (BM-SC-CRC1, BM-SC-CRC2, BM-SC-CRC3, and

**Table 1.** Clinical Characteristics of Patients From Whom BM-SC-CRC Were Derived

|  | Patient 1 | Patient 2 | Patient 3 | Patient 4 |
| --- | --- | --- | --- | --- |
| Age (y) | 54 | 70 | 64 | 53 |
| Gender | Male | Male | Female | Female |
| Primary tumor location | Rectum | Sigmoid | Colon | Rectum |
| BM location | Right frontal lobe | Right frontal lobe | Posterior fossa | Right frontal lobe |
| BM number | 2 | 1 | 1 | 2 |
| Delay between primary tumor and BM diagnosis (mo) | 59 | 18 | 42 | 0 |
| No. of lines of chemotherapy before BM diagnosis | 4 | 1 | 2 | 3 (breast cancer) |
| Chemotherapy in the month before BM diagnosis | Yes | No | No | No |
| Metastatic sites before BM diagnosis | Liver, lung, bone | None | Liver, lung | Node, liver, bone, lung |
| Treatment after BM surgery | Palliative care | Radiotherapy (surgical site) | Radiotherapy (surgical site) | Radiotherapy (surgical site) and chemotherapy |
| Progressive disease after BM diagnosis (sites) | No imaging | Brain | No imaging | No imaging |
| Survival after BM diagnosis (mo) | 4 | 6 | 3 | 8 |
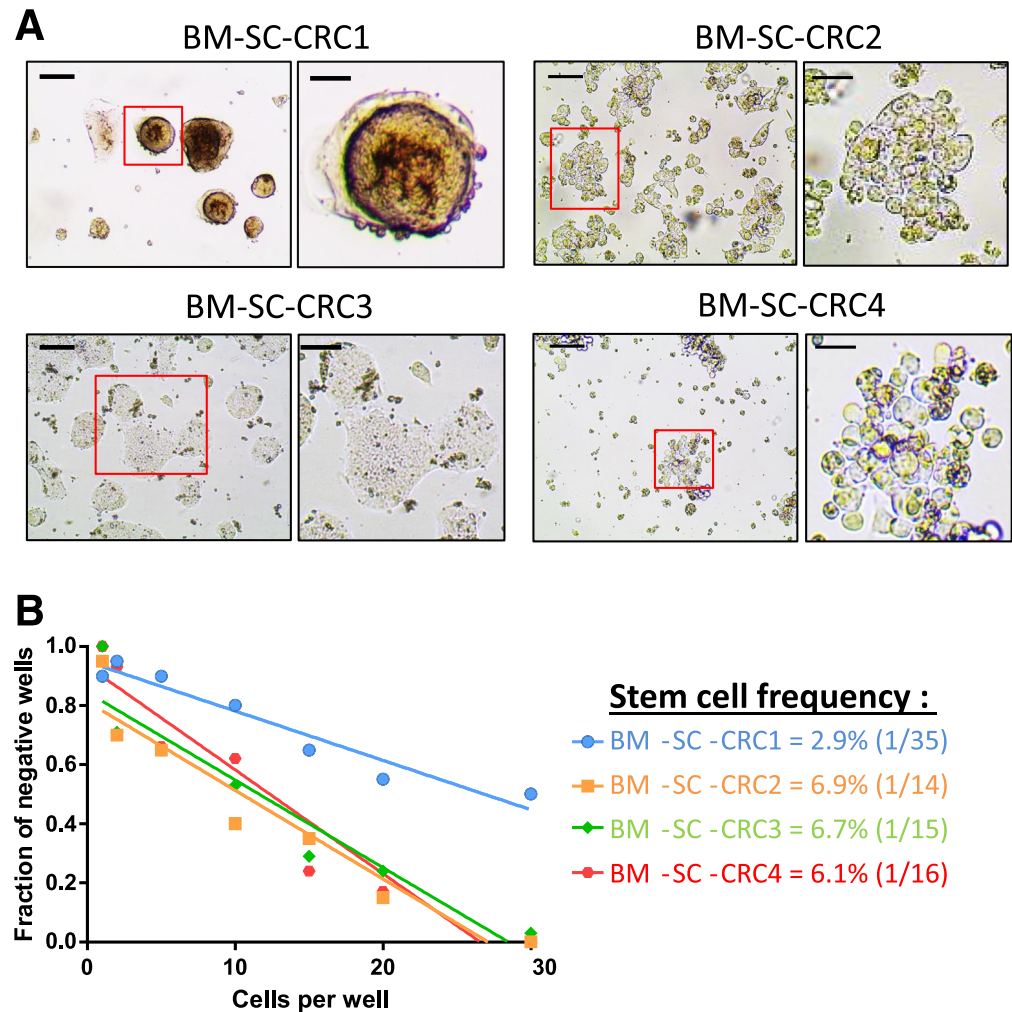
**Figure 1. BM-SC-CRCs containing cancer stem-like cells and form metaspheres.** (*A*) BM-SC-CRC cells in stem cell culture condition DMEM/F12 medium enriched with bFGF and EGF. Representative photography ×40 (scale bar, 50 μm) and zoom (scale bar, 10 μm). (*B*) Limiting dilution analysis. Poisson distribution was used to determine the dilution at which one single stem cell would give rise to a single metasphere, estimating stem cell frequency ($F0 = e-x$ when $x = 1$ and $F0 = 0.37$).

BM-SC-CRC4). After 5 cell passages some cells started to grow semi-adherently. To ascertain the self-renewal ability and clonogenicity of these cells, clonogenic assay with a semisolid matrix enriched with growth factors was performed and showed that clonogenic efficiencies were 9.1% for BM-SC-CRC1, 12.7% for BM-SC-CRC2, 15.5% for BM-SC-CR3, and 27.9% for BM-SC-CRC4 (Figure 2). To evaluate the frequency of metasphere initiating cells, which reflects the frequency of a stem cell population, we conducted limiting dilution assays. We observed that the frequencies were 1 of 35 (2.9%) for BM-SC-CRC1, 1 of 14 (6.9%) for BM-SC-CRC2, 1 of 15 (6.7%) for BM-SC-CRC3, and 1 of 16 (6.1%) for BM-SC-CRC4 (Figure 1B).

## BM-SC-CRC Lines Express Stem Cell Markers and Are Able to Differentiate

We found by Western blot and immunofluorescence analysis that all 4 BM-SC-CRC lines strongly express CD44, EpCAM, CD133, Lgr5, and ALDH1, which are CRC stem cell markers[12,16,17,20] (Figures 3A and B and 4A). Interestingly all cells also expressed CD44v6, which is known to be specifically associated with CSC presenting metastatic potential in CRC. We also observed that BM-SC-CRC lines were able to differentiate when they were seeded in a medium supplemented with fetal bovine serum (FBS). After 7 days of culture, cells presented a polygonal shape shift and were growing adherently. In these conditions, cells expressed epithelial markers such as CK20 and CK19 as well as CDX2, a critical nuclear transcription factor for intestinal development, which is expressed in differentiated intestinal epithelium and CRC (Figures 3C and D and 4B). Moreover, we found that stem cell markers were also affected after serum treatment (Figures 3B and 5). It is now known that cancer stem cell plasticity and heterogeneity are very complex, and this metastable phenotype could effectively explain the existence of differentiation markers in "stem condition" and vice versa.[26]

## BM-SC-CRC Lines Have Invasive and Migratory Capabilities in an In Ovo Model

We used the chicken embryos chorioallantoic membrane (CAM) assay to study the tumor growth, the invasive ability,
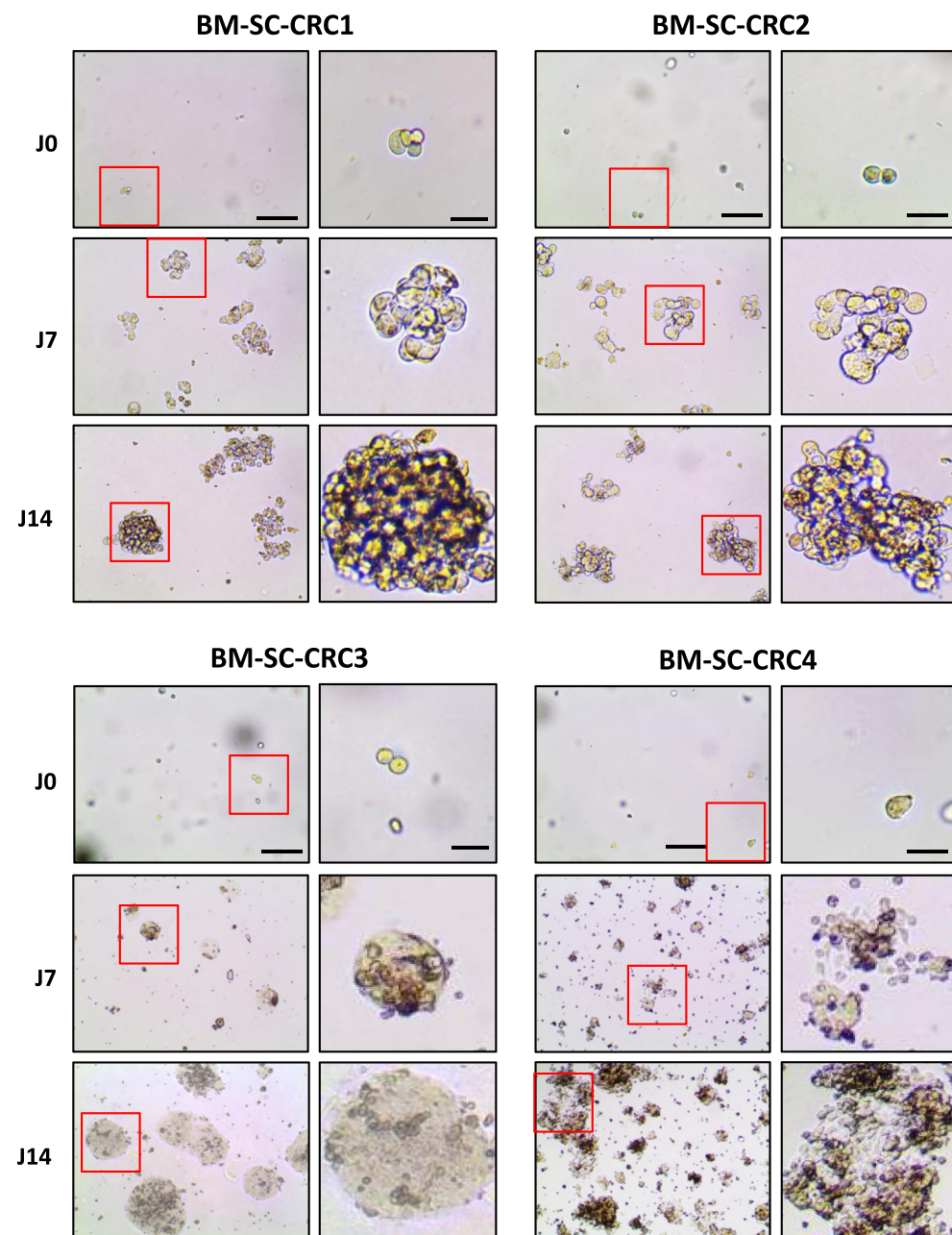
**Figure 2. Self-renewal ability and clonogenicity of metasphere in methylcellulose of BM-SC-CRC lines.** After 14 days of culture of 40,000 cells, metasphere forming units were determined for each cell line, and plating efficiency (PE) was calculated (colonies number divided by number of cells plated). Representative photography ×10 (scale bar, 100 μm) and zoom (scale bar, 20 μm).
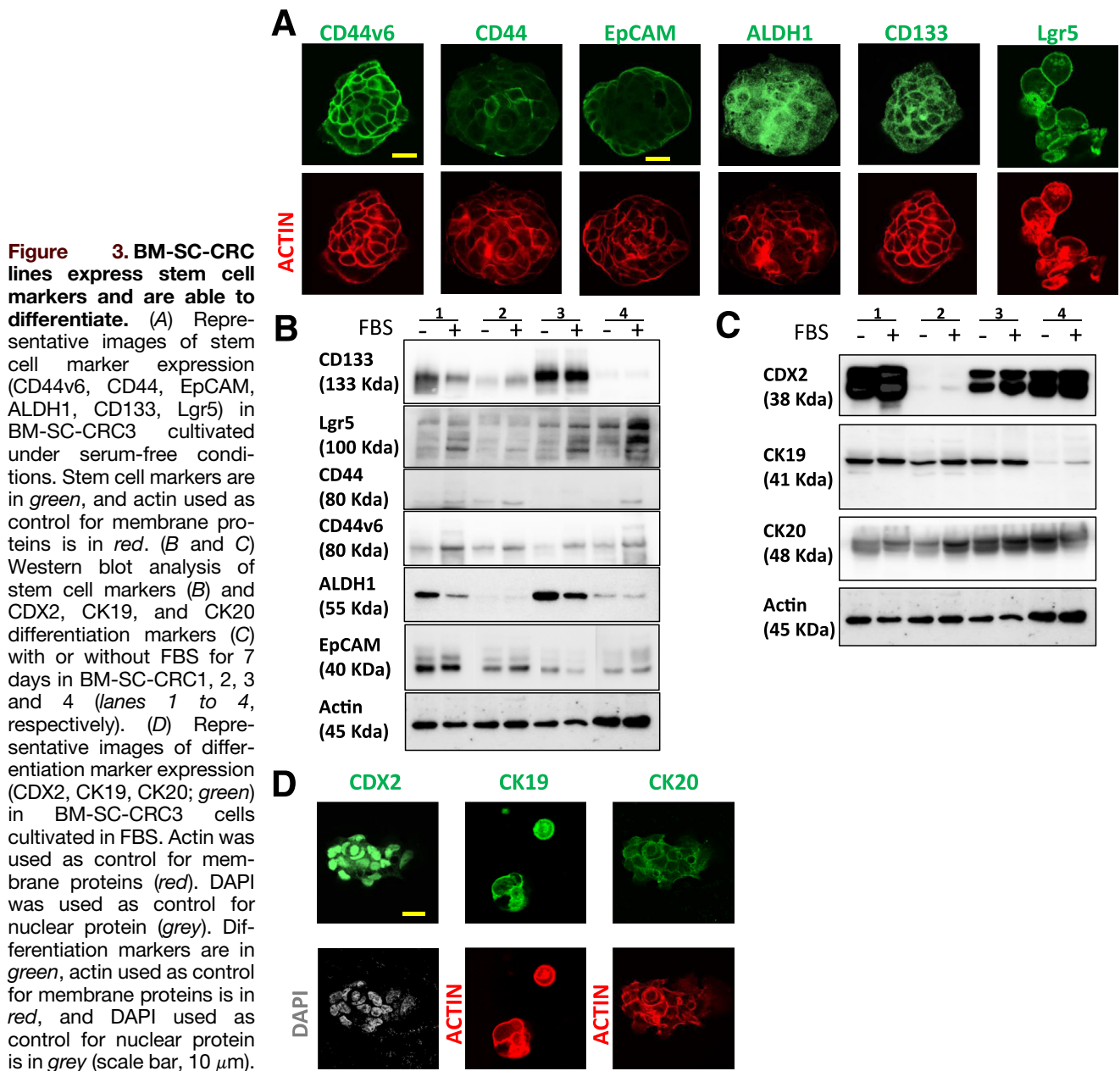
PE : BM-SC-CRC1 = 9.1 % - BM-SC-CRC2 = 12.7 % - BM-SC-CR3 = 15.5 % - BM-SC-CRC4 = 27.9 %

and angiogenesis of patient-derived BM-SC-CRC1 and 2 cell lines (Figure 6A). After grafting of 3 million cells on the CAM of 25 eggs for each cell line and an incubation period of 9 days, the mean tumor weight for BM-SC-CRC1 (n = 25) and BM-SC-CRC2 (n = 19 survivor embryos) cell lines was comparable with 15.54 and 14.55 mg, respectively (Figure 6B). BM-SC-CRC cell lines were invasive with a relative metastasis quantity of 5% and 3% for BM-SC-CRC1 and BM-SC-CRC2, respectively, compared with negative control group (n = 8, Figure 6C). Concerning angiogenesis, a good vessel development was observed, with a mean value of 52 and 49.2 vessels colonizing the tumor for BM-SC-CRC1

(n = 11) and 2 (n = 10), respectively (Figure 6D). Taken together, our results showed that both cell lines, which also expressed CD44v6 (Figure 3A and B), were invasive with migratory capabilities.

### BM-SC-CRC Lines Recapitulate Patient's Brain Metastasis Features After Intracranial Injection in Immunocompromised Mice

To ascertain the tumorigenicity of BM-SC-CRC lines, we assessed their tumor formation capacity after intracranial injection into the striatum of immunocompromised mice

**Figure 3. BM-SC-CRC lines express stem cell markers and are able to differentiate.** (*A*) Representative images of stem cell marker expression (CD44v6, CD44, EpCAM, ALDH1, CD133, Lgr5) in BM-SC-CRC3 cultivated under serum-free conditions. Stem cell markers are in *green*, and actin used as control for membrane proteins is in *red*. (*B* and *C*) Western blot analysis of stem cell markers (*B*) and CDX2, CK19, and CK20 differentiation markers (*C*) with or without FBS for 7 days in BM-SC-CRC1, 2, 3 and 4 (*lanes 1 to 4*, respectively). (*D*) Representative images of differentiation marker expression (CDX2, CK19, CK20; *green*) in BM-SC-CRC3 cells cultivated in FBS. Actin was used as control for membrane proteins (*red*). DAPI was used as control for nuclear protein (*grey*). Differentiation markers are in *green*, actin used as control for membrane proteins is in *red*, and DAPI used as control for nuclear protein is in *grey* (scale bar, 10 μm).

(n = 12). Mice were killed after 10% loss of body weight in 24 hours, and we observed that the BM-SC-CRC allowed the formation of large tumoral masses in brain (Figures 7A,8A, 9A, and 10A). Tumor formation was detected after 12 weeks for BM-SC-CRC1, 8 weeks for BM-SC-CRC2 and BM-SC-CRC3, and 4 weeks for BM-SC-CRC4. The histologic analysis of xenograft tumors showed colorectal adenocarcinoma characteristics recapitulating the original patient BM histology (Figures 7B, 8B, 9B, and 10B). The brain tumors from BM-SC-CRC lines were CDX2+/CK20+ identically to the original patient BMs (Figures 7C, 8C, 9C, and 10C). Finally, the serial intracranial injection confirmed BM-SC-CRC self-renewal capacity in vivo (Figure 11).

## Molecular Characterization of BM-SC-CRC Highlights Shared Genetic Variations and Expression Signatures

A molecular characterization of patient-derived BM-SC-CRC cell lines, BM, and primary tumor samples was performed by whole exome sequencing. First, we focused on a restricted gene panel including clinically relevant genes such as *RAS, BRAF,* and *PIK3CA* (Table 2). For patient 1, no significant somatic mutations were found. For patient 2, we identified 2 pathogenic variations, namely *KRAS* p.(Gly12Ser) and *PIK3CA* p.(Glu542Lys), in BM-SC-CRC2 as well as in patient's BM and primary tumor. In the same way for patient 3, we found *KRAS* p.(Gly13Asp) mutation in all
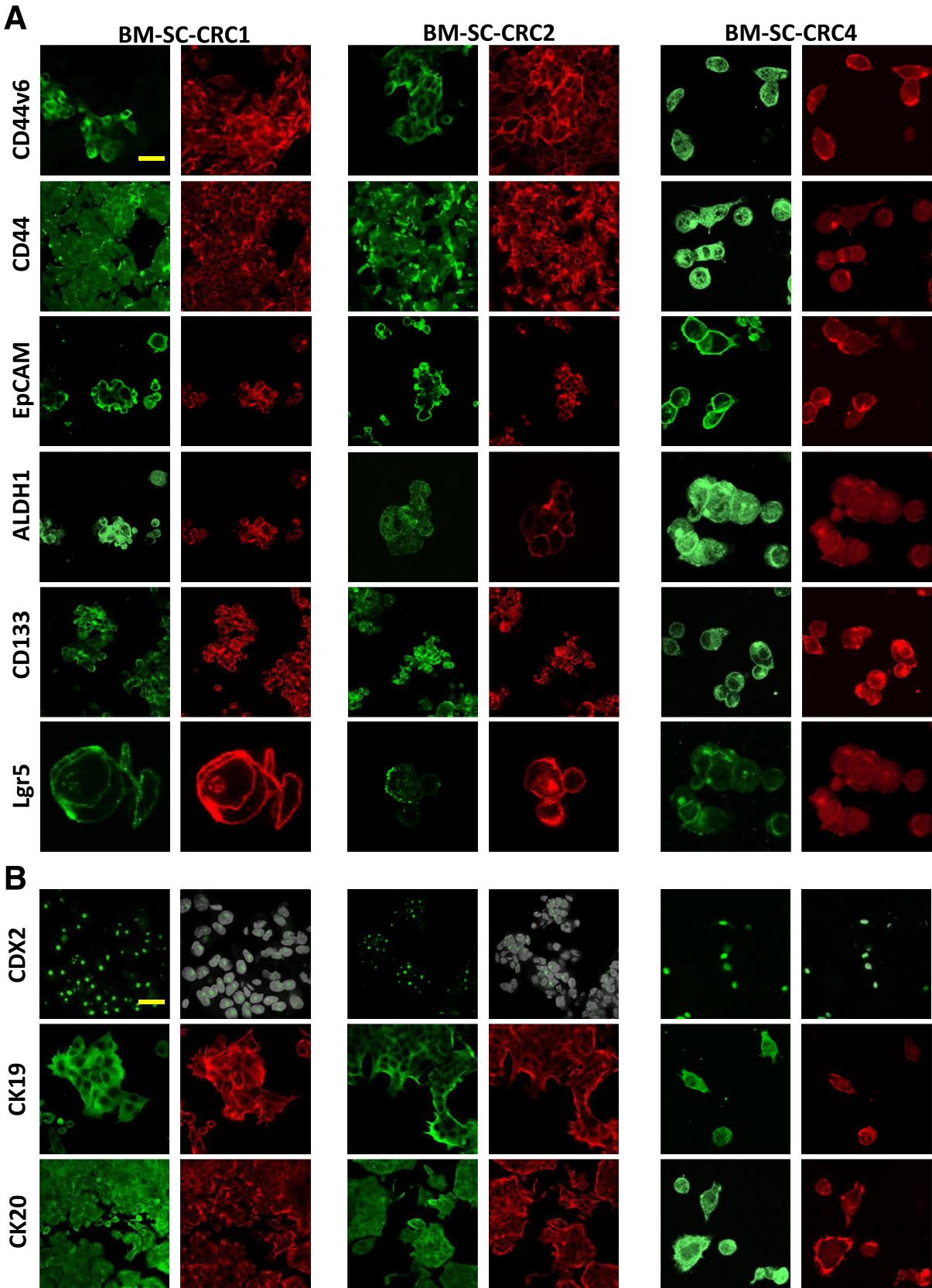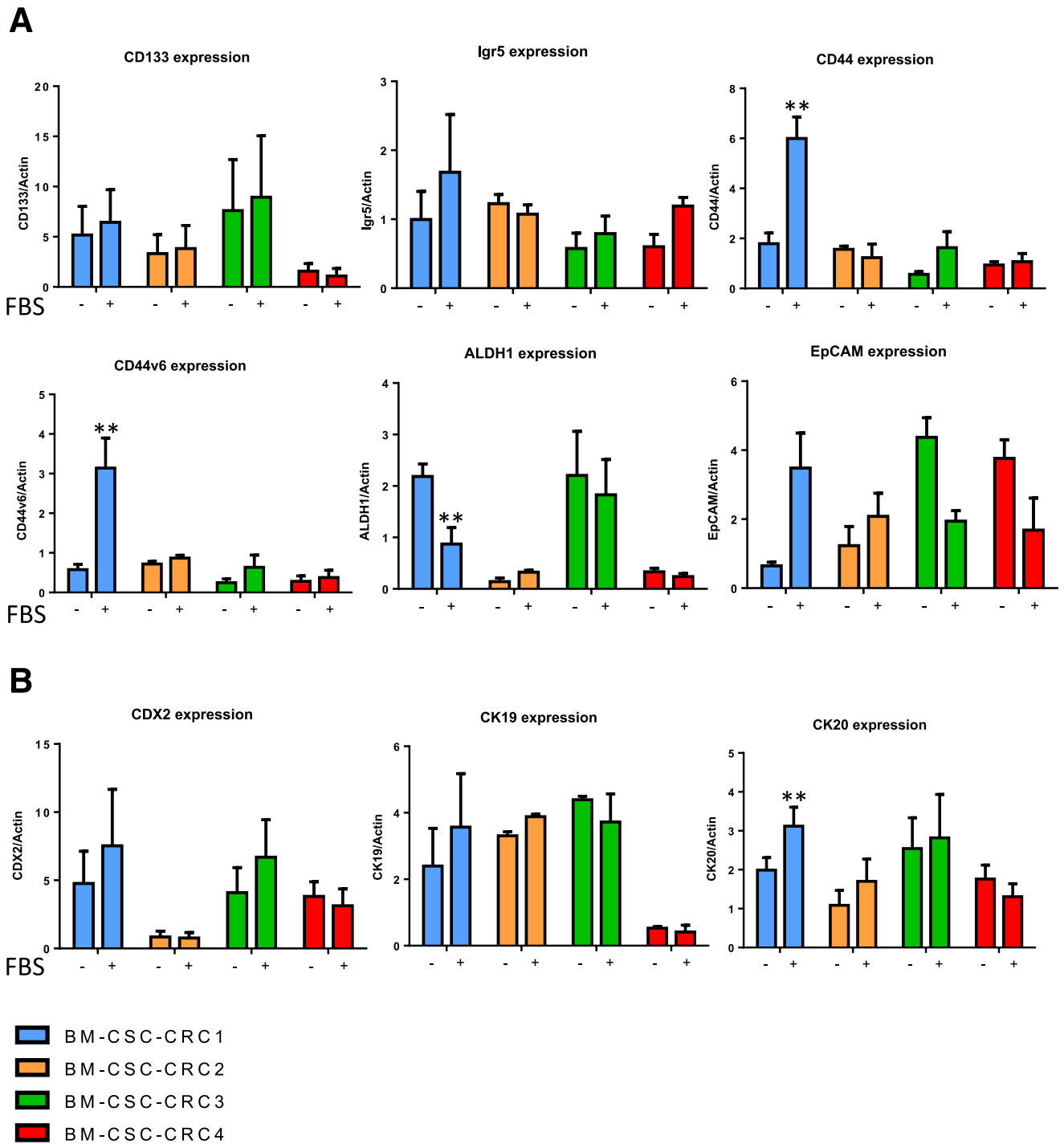
**Figure 5.** **Western blot quantification of stem cell and differentiation markers on BM-SC-CRC.** (*A* and *B*) Western blot quantification of stem cell markers (*B*) and CDX2, CK19, and CK20 differentiation markers (*C*) with or without FBS for 7 days in BM-SC-CRC1, 2, 3, and 4 (*lines 1 to 4*, respectively). \*\**P* < .01, two-way analysis of variance.

---

**Figure 4.** (*See previous page*). **Immunofluorescence of stem cell and differentiation markers on BM-SC-CRC.** (*A* and *B*) Representative images of stem cell marker expression (CD44v6, CD44, EpCAM, ALDH1, CD133, Lgr5; *green*) in BM-SC-CRC1, 2, and 4 cultivated under serum-free conditions (*A*) and differentiation markers (CDX2, CK19, CK20; *green*) in BM-SC-CRC1, 2, and 4 cultivated in FBS. Actin is used as control for membrane proteins (*red*). DAPI is used as control for nuclear protein (*grey*). (Scale bar, 10 $\mu$m).
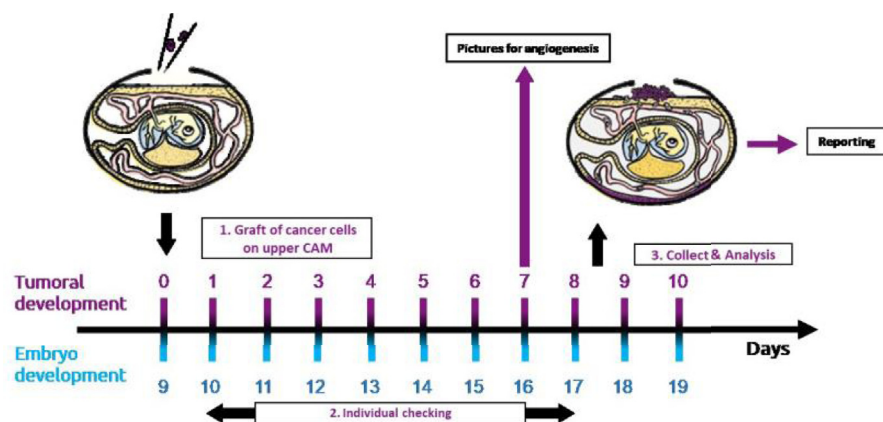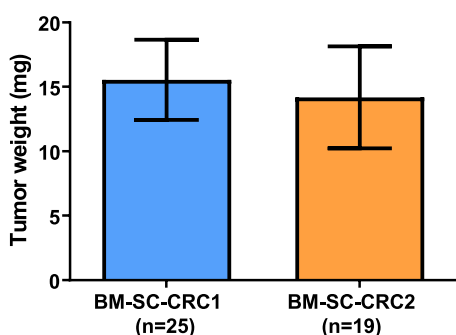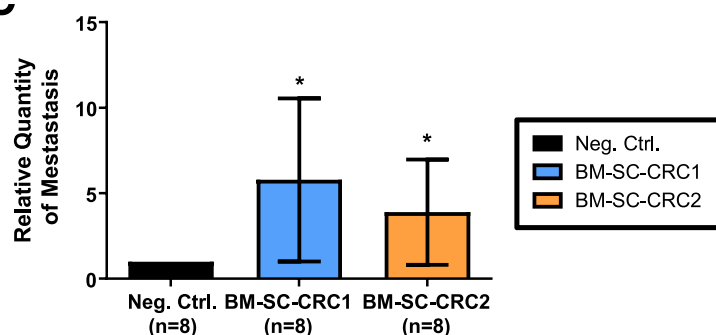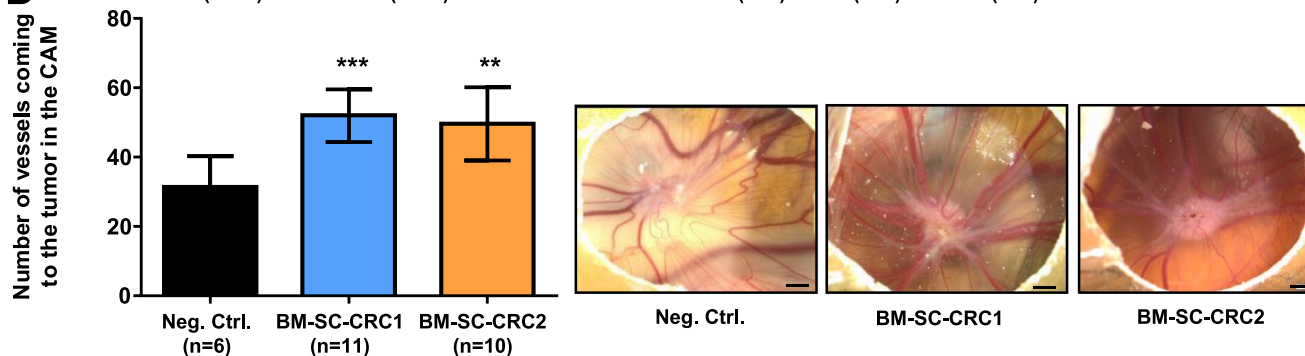
**Figure 6. In ovo model showing invasive and migratory abilities of BM-SC-CRC1-2.** (*A*) In ovo experimental approach with BM-SC-CRC cells. (*B*) On E18 day, tumors are cut away from normal CAM tissue and weighed (n = 8). (*C*) On day E18, a portion of the lower CAM is collected to evaluate the number of metastatic cells in 8 samples per group (n = 8). Genomic DNA is analyzed by quantitative polymerase chain reaction with specific primers for Human Alu sequences. (*D*) On day E16, a picture of the upper CAM (with tumor) is taken. The number of blood vessels that reach the tumor is counted to evaluate tumor angiogenesis (n = 6). Scale bar, 1 mm. Samples number are directly indicated in the panels. *$P < .05$, **$P < .01$, ***$P < .001$ compared with negative control (Neg. Ctrl.). Grubb's tests.

samples. For patient 4 we identified the *NRAS* p.(Gln61Arg) mutation in the BM and its derived BM-SC-CRC4 lines but not in the primary tumor. Finally, we found that all BM-SC-CRC cell lines and tumor samples presented an MSS phenotype.

Then, to better characterize our patient-derived cell lines and to identify new potential variations of interest, a molecular characterization was performed on 89 genes presenting a mutation rate of more than 3% in mCRC, according to TCGA and MSKCC studies available at cBioPortal (https://www.cbioportal.org). We found that variant classification

and type were mainly represented by missense mutations and single nucleotide polymorphism in primary tumors, BM, and derived BM-SC-CRC for all patients (Figure 12*A*). Moreover, the single nucleotide variant class showed that the main variation is T>C and C>T for all patients. We also observed that the number of variations in patients 1 and 3 is higher in primary tumors than BM and BM-SC-CRC, whereas patient 2 showed a higher variation in BM and derived cell line than in primary tumor as for patient 4. However, it is important to note that DNA extraction from patient 4 primary tumor was very low. Interestingly, the top 10 mutated
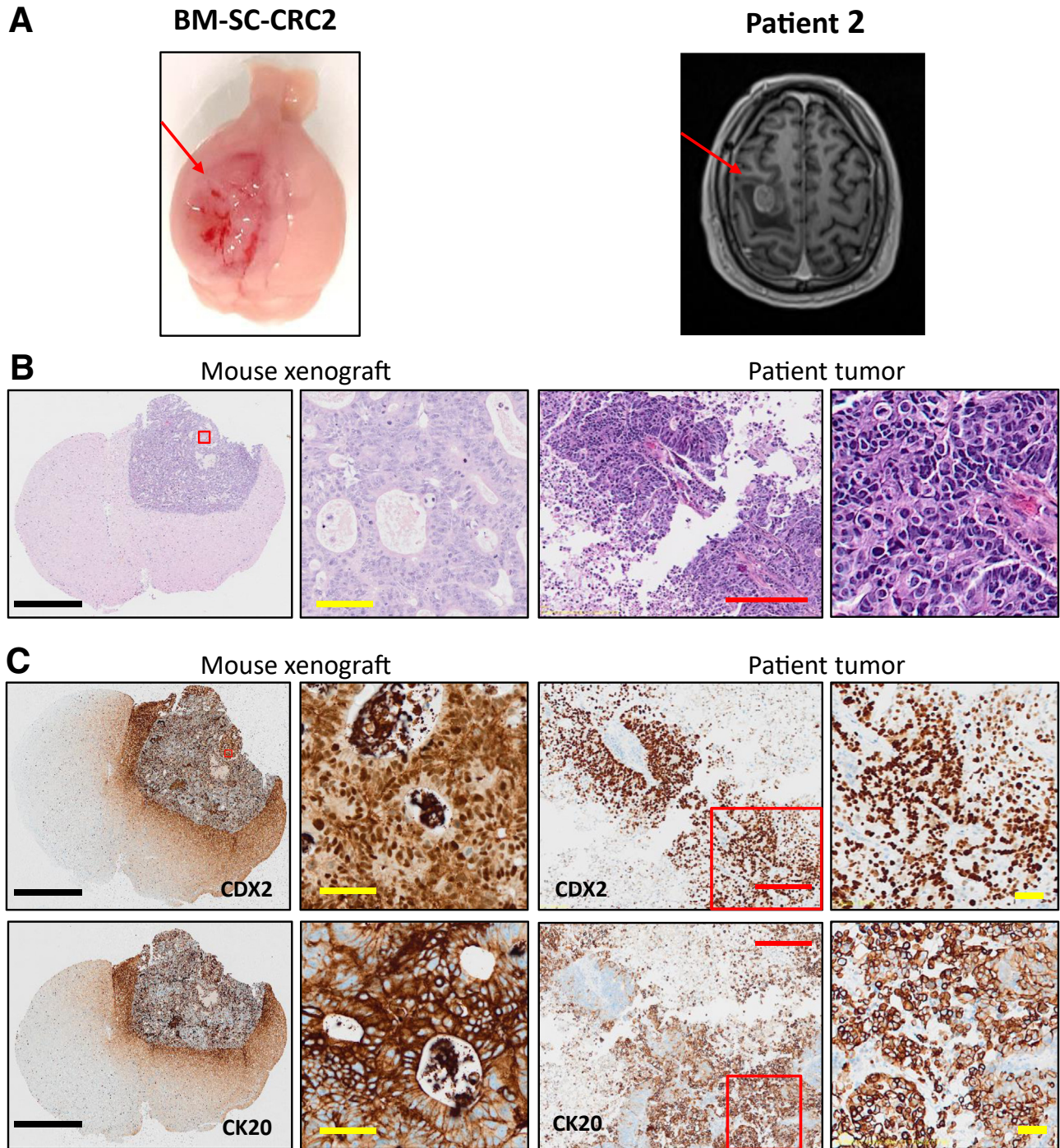
**Figure 7. Intracranial injections of BM-SC-CRC2 lines in immunocompromised mice recapitulate patient's BM features.** (*A*) Representative image of BM-SC-CRC2 xenograft after 8 weeks (*left panel*, *red arrow*) and patient 2 MRI before surgery (*right panel*, *red arrow*). (*B*) Hematoxylin/eosin staining of mouse xenograft and corresponding patient tumor. (C) CDX2 and CK20 immunostaining of mouse xenograft and corresponding patient tumor observed at low and high magnification. (*Black scale bar*, 200 μm; *yellow scale bar*, 10 μm; *red scale bar*, 50 μm).

genes revealed that *KMT2C*, *KMT2D*, *ARID1A,* and *ZFHX3* represent the most affected genes in all samples. Then, we determined the intersection between the different genes and variants among primary tumors, BMs, and patient-derived cell lines and found that several genes and variants are present along tumoral evolution (Figure 12B,

Table 3). We detected 55% and 27% ubiquitous variations for patients 2 and 3, respectively. For patient 1, there is a high rate of mutations identified only in primary tumor, and only 4% are ubiquitous in the 3 samples. For patient 4, there is no ubiquitous variation because DNA extracted from primary tumor was non-contributive. In addition, we
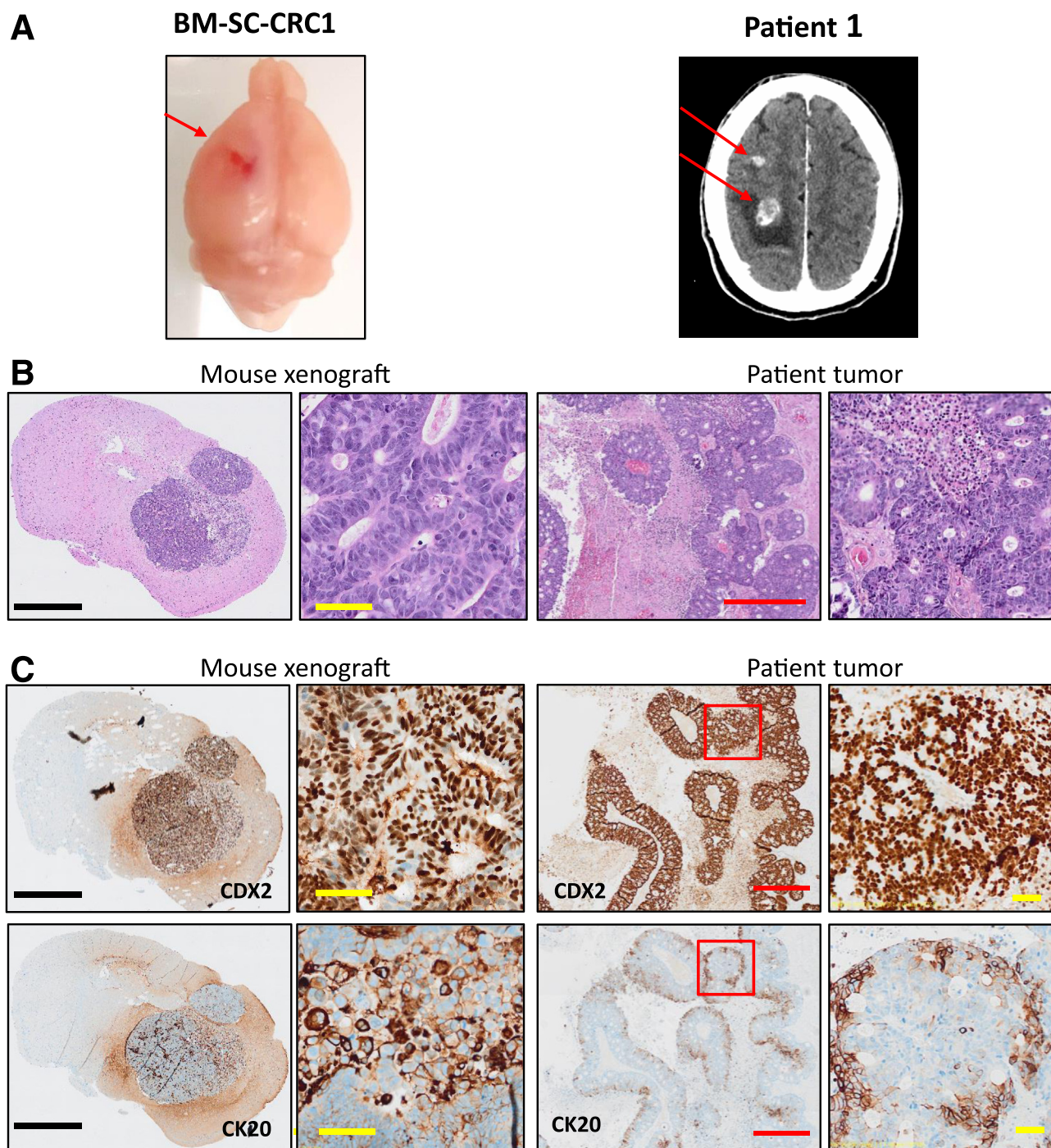
**Figure 8. Intracranial injections of BM-SC-CRC1 lines in immunocompromised mice recapitulate patient's BM features.** (*A*) Representative image of BM-SC-CRC1 xenograft after 12 weeks (*left panel, red arrow*) and patient 1 magnetic resonance imaging before surgery (*right panel, red arrow*). (*B*) Hematoxylin/eosin staining of mouse xenograft and corresponding patient tumor. (*C*) CDX2 and CK20 immunostaining of mouse xenograft and corresponding patient tumor observed at low and high magnification. (*Black scale bar*, 200 $\mu$m; *yellow scale bar*, 10 $\mu$m; *red scale bar*, 50 $\mu$m).

observed 23%, 29%, 62%, and 62% of shared variations between BM and its derived cell line in patients 1 to 4, respectively (Figure 12*B*). Moreover, 8 *KMT2C* and 1 *ZFHX3* variants are common between patients with a stable variant allele frequency from primitive to patient-derived stem cells (Table 3). Then, we focused our attention on patient-derived

cell lines in which some mutated genes could potentially play a pivotal role in BM formation and progression. All BM-SC-CRCs showed a majority of missense mutations, single nucleotide polymorphism variations and presented multihit mutations. Thirty-four mutated genes belonging to onco-genic signaling pathways such as RTK-Ras, PI3K, Notch,
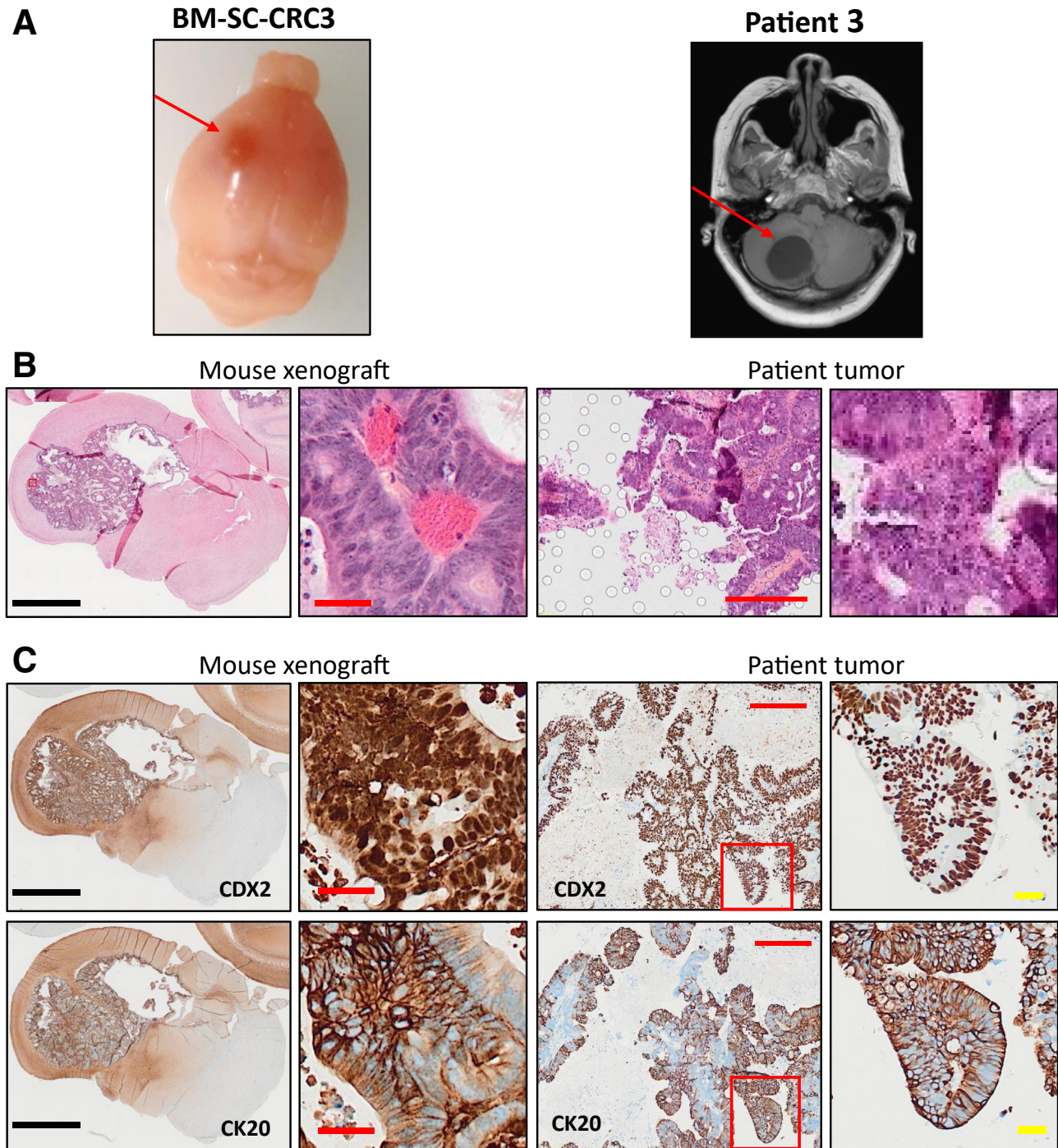
**Figure 9. Intracranial injections of BM-SC-CRC3 lines in immunocompromised mice recapitulate patient's BM features.** (*A*) Representative image of BM-SC-CRC3 xenograft after 8 weeks (*left panel, red arrow*) and patient 3 magnetic resonance imaging before surgery (*right panel, red arrow*). (*B*) Hematoxylin/eosin staining of mouse xenograft and corresponding patient tumor. (*C*) CDX2 and CK20 immunostaining of mouse xenograft and corresponding patient tumor observed at low and high magnification. (*Black scale bar*, 200 $\mu$m; *yellow scale bar*, 10 $\mu$m; *red scale bar*, 50 $\mu$m).

Wnt, and Hippo are altered in all BM-SC-CRC and transforming growth factor $\beta$ pathway in 3 BM-SC-CRC (Figure 13*D*). Among the top 10 mutated genes, *KMT2C/D, ARID1A, CREBBP,* and *ZFHX3* are the genes with the higher frequency of variations for all BM-SC-CRC (Figure 13*A* and *B*), and 16 variants corresponding to 5 different genes are

common between BM-SC-CRC (Supplementary Table 1). By analyzing the expression of the 89 genes from RNASeq data of BM-SC-CRC, we found that mutation rate seems to be correlated to gene expression (Figure 13*B* and *C*). More interestingly, we found that 19 mutated genes appear as druggable categories, and some of them are clinically
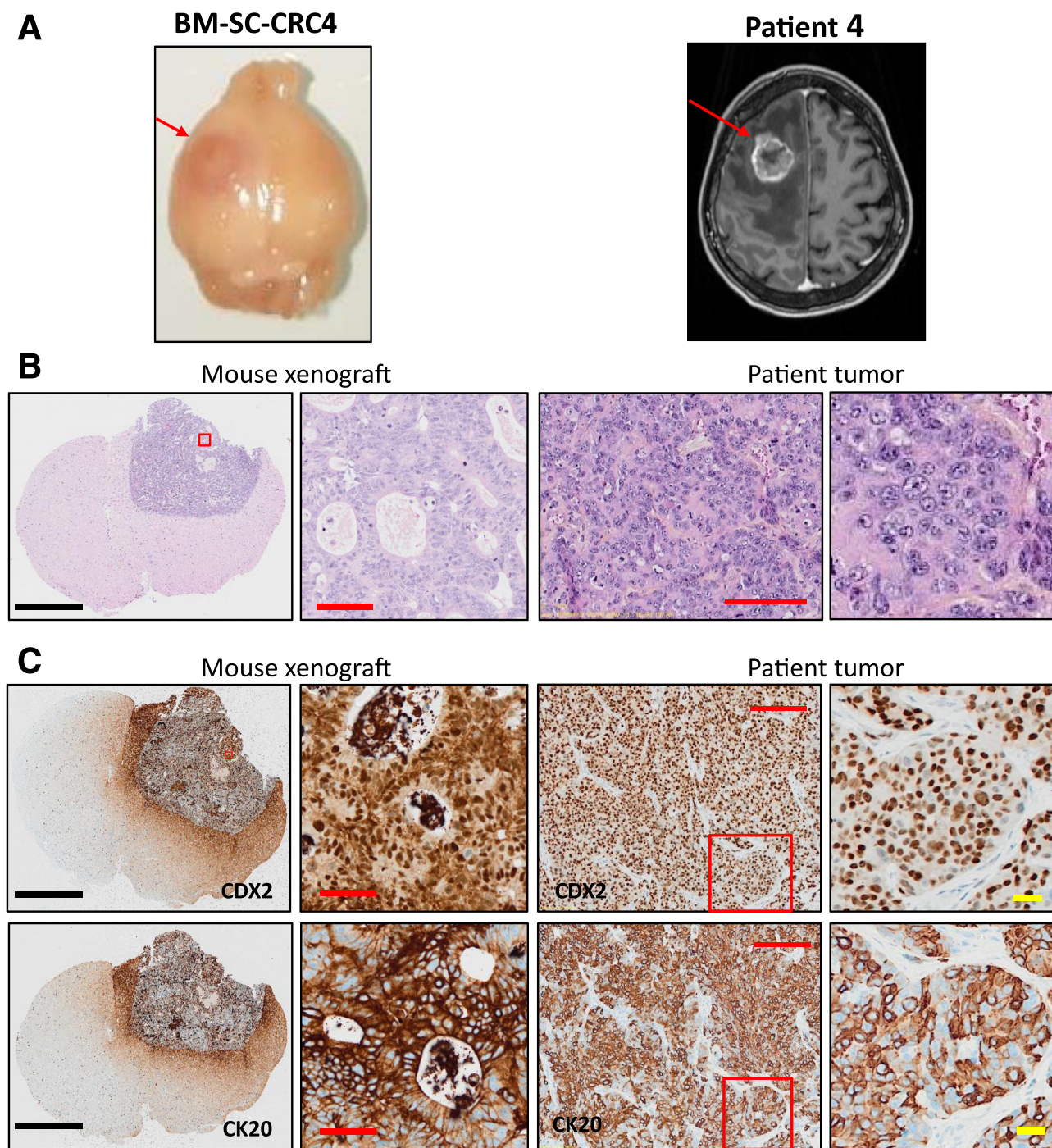
**Figure 10. Intracranial injections of BM-SC-CRC4 lines in immunocompromised mice recapitulate patient's BM features.** (*A*) Representative image of BM-SC-CRC4 xenograft after 4 weeks (*left panel, red arrow*) and patient 4 magnetic resonance imaging before surgery (*right panel, red arrow*). (*B*) Hematoxylin/eosin staining of mouse xenograft and corresponding patient tumor. (*C*) CDX2 and CK20 immunostaining of mouse xenograft and corresponding patient tumor observed at low and high magnification. (*Black scale bar*, 200 μm; *yellow scale bar*, 10 μm; *red scale bar*, 50 μm).

actionable especially *KMT2* family (Figure 13*E*, Table 4). Finally, we found by compiling our data that *KMT2C* c.2961C>G /p.(Tyr987ter) variant are the only one common from primary tumor to metastasis and cell lines, clinically actionable, and described as pathogenic by generating a stop codon in Zinc finger domain of the protein (Figure 13*F*).

KMT2C, also known as MLL3, could represent a new potential candidate for further investigation in CRC BM dissemination.

To further study biological processes and signaling pathways, which could be specifically expressed in BM-SC-CRC, we performed a differential transcriptomic analysis
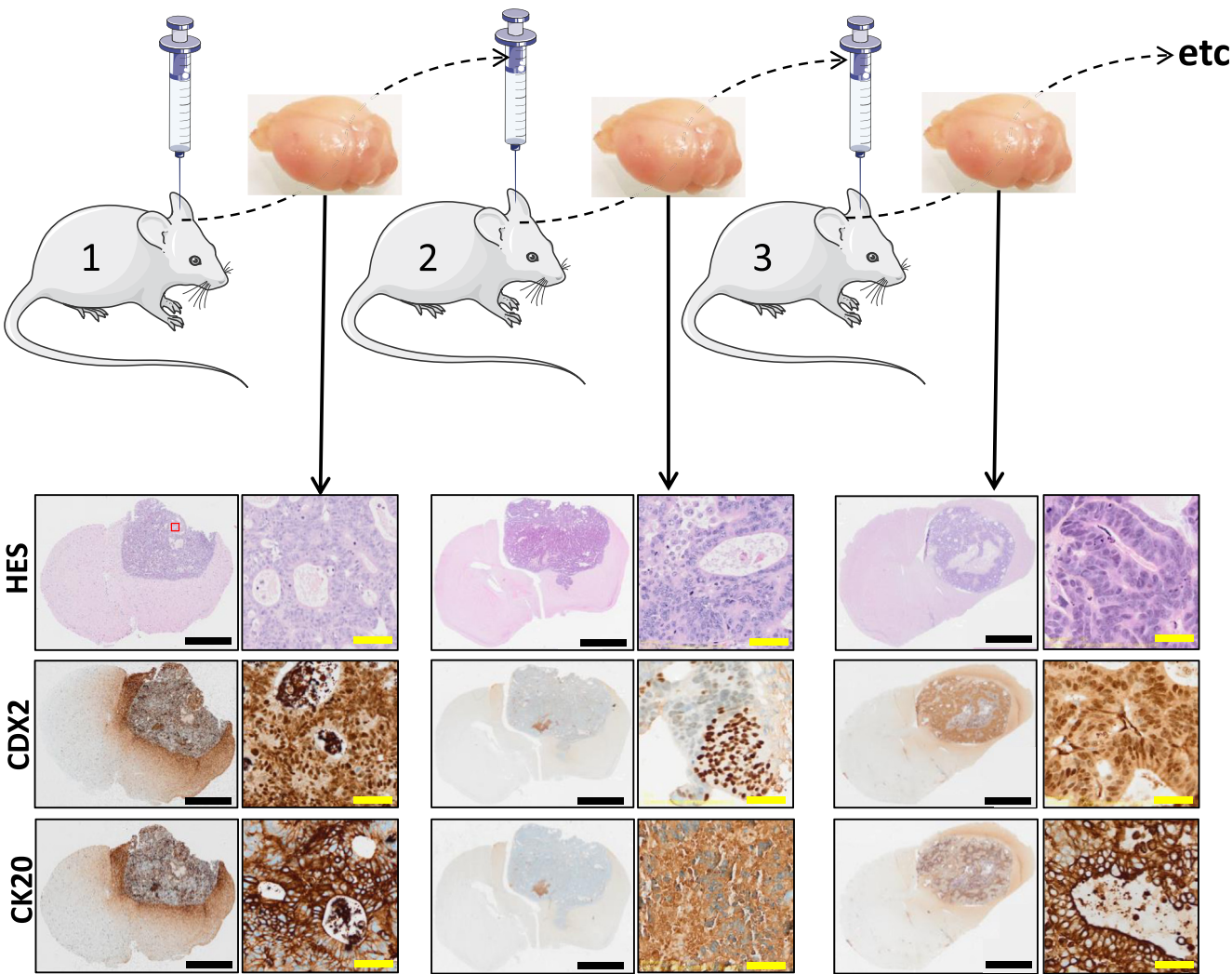
**Figure 11. Serial transplantation of BM-SC-CRC2 cell line.** Representative image of BM-SC-CRC2 xenografts after serial transplantation showing self-renewal capacity in vivo with conservation of histologic features and CDX2/CK20 positivity. For this cell line, about 8 weeks are necessary to develop intracranial tumor. Tumor was dissociated and injected to next mice immediately. Delay between intracranial injection and tumor development is patient cell line dependent. (*Black scale bar*, 200 $\mu$m; *yellow scale bar*, 10 $\mu$m).

**Table 2.** Molecular Characteristics of Patients From Whom BM-SC-CRC Were Derived

|  | Patient 1 | Patient 2 | Patient 3 | Patient 4 |
|---|---|---|---|---|
| Microsatellite instability status | MSS | MSS | MSS | MSS |
| Clinically significant variant (found in primary tumor and BM) | None | KRAS: c.34G>A / p.(Gly12Ser) PIK3CA: c.1624G>A / p.(Glu542Lys) | KRAS: c.38G>A / p.(Gly13Asp) | NRAS: c.182A>G / p.(Gln61Arg) (present in BM but not in primary tumor) |

NOTE. Molecular characteristics performed with a restricted panel with clinically relevant genes (AKT1, ALK, BRAF, EGFR, ERBB2, ERBB4, FGFR2, FGFR3, H3F3A, HIST1H3B, HRAS, IDH1, IDH2, KIT, KRAS, MAP2K1, MET, NRAS, PDGFRA, PI3KCA), microsatellite instability status.
BM, brain metastasis; MSS, microsatellite stability.
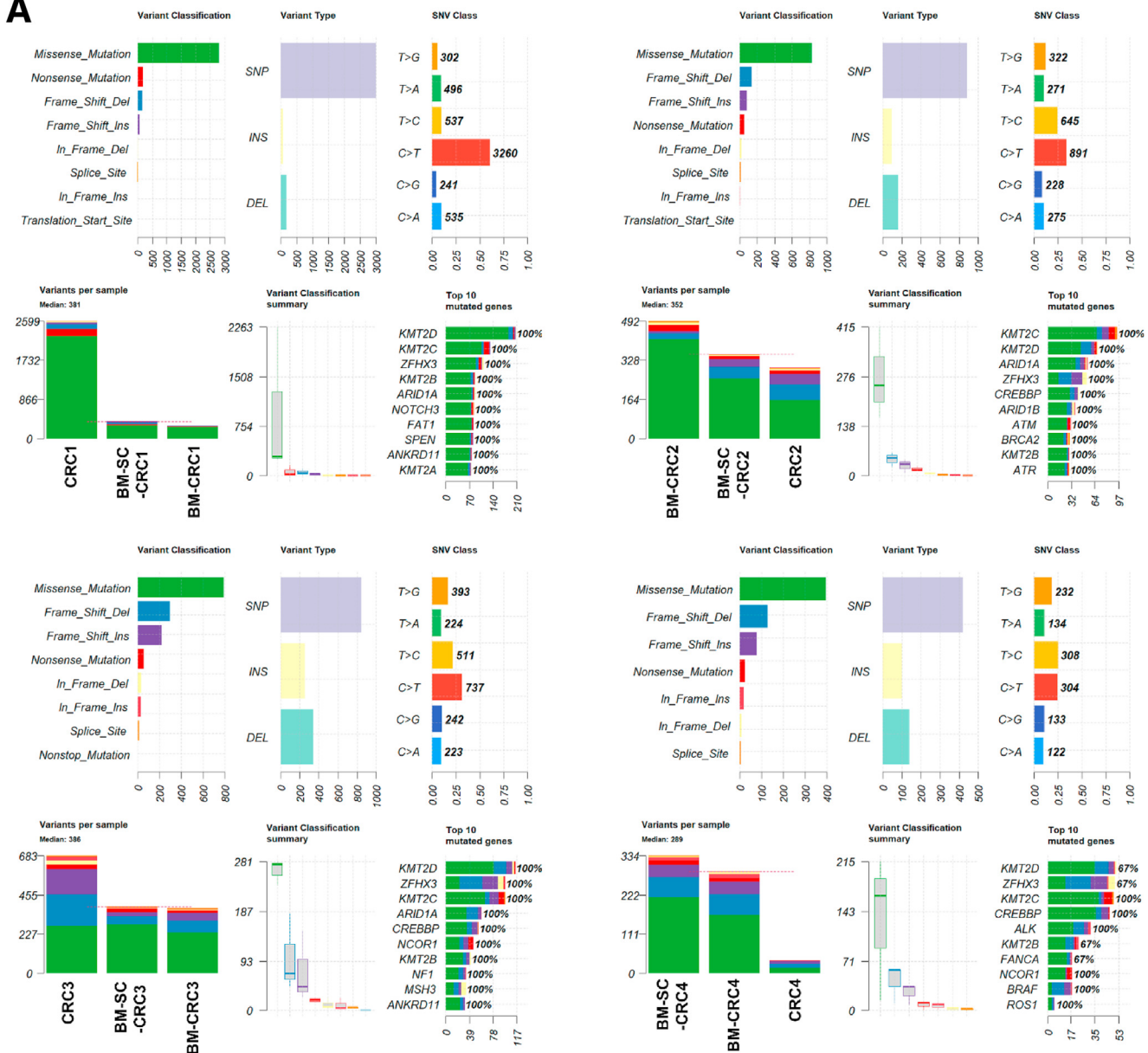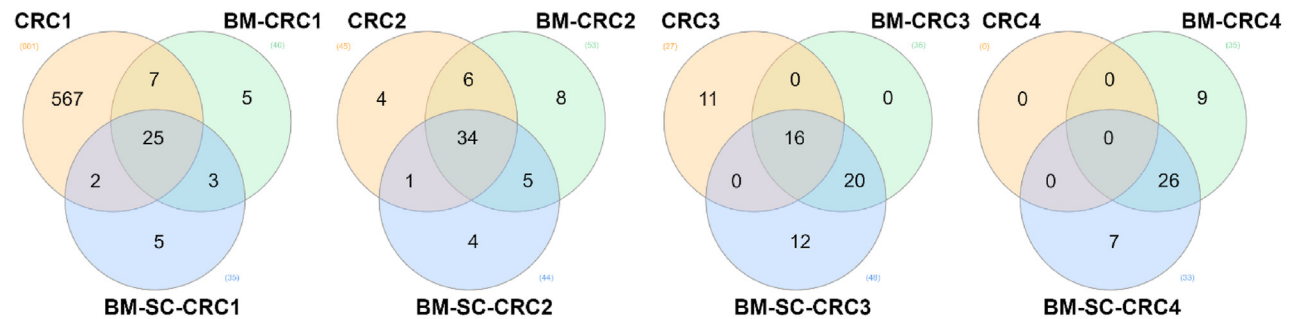
**Figure 12. Whole exome sequencing (WES) analysis of primary CRC tumors, BM, and associated BM-SC-CRC cell lines.** (*A*) Summary of WES analysis from 89 genes highlighting variant classification and type, SNV class, and top 10 mutated genes for the 3 sample types (primary tumor, CRC; brain metastasis, BM-CRC; stem cell line derived from brain metastasis, BM-SC-CRC) for each patient. (*B*) Venn diagram showing the number of common variants between the 3 sample types for each patient. DEL, deletion; INS, insertion; SNP, single nucleotide polymorphism; SNV, single nucleotide variant; TMB, tumor mutational burden.

**Table 3.** Ubiquitous and Shared Variations for Primary Tumors, Brain Metastases, and Derived Cell Lines

| | Gene | nt_change | aa_change | VAF_Primitive | VAF_Metastasis | VAF_Stem_cells | Effect | Impact |
|---|---|---|---|---|---|---|---|---|
| CRC1 | KMT2C | c.2573G>T | p.Trp858Leu | 0.40447155 | 0.47938144 | 0.23786408 | Missense_variant | Variant of unknown significance |
| CRC1 | KMT2C | c.2578C>T | p.Pro860Ser | 0.39626168 | 0.45686901 | 0.21875 | Missense_variant | Variant of unknown significance |
| CRC1 | KMT2C | c.2726G>A | p.Arg909Lys | 0.17605634 | 0.11309524 | 0.1344086 | Missense_variant | Variant of unknown significance |
| CRC1 | KMT2C | c.2917A>G | p.Arg973Gly | 0.14313197 | 0.25927688 | 0.15662651 | Missense_variant | Variant of unknown significance |
| CRC1 | KMT2C | c.2961C>G | p.Tyr987X | 0.14464383 | 0.23649078 | 0.13965087 | stop_gained | Pathogenic |
| CRC1 | KMT2C | c.2963G>T | p.Cys988Phe | 0.63083849 | 0.7097429 | 0.60606061 | Missense_variant | Variant of unknown significance |
| CRC1 | KMT2C | c.871C>T | p.Leu291Phe | 0.66261398 | 0.54505972 | 0.57509881 | Missense_variant | Variant of unknown significance |
| CRC1 | KMT2C | c.946A>T | p.Thr316Ser | 0.80505254 | 0.74781225 | 0.72968349 | Missense_variant | Variant of unknown significance |
| CRC1 | ZFHX3 | c.2330T>C | p.Val777Ala | 0.994709 | 0.99546828 | 0.99331104 | Missense_variant | Benign |
| | Gene | nt_change | aa_change | af_Primitive | af_Metastasis | af_Stem_cells | Effect | Impact |
| CRC2 | KMT2C | c.2573G>T | p.Trp858Leu | 0.29145729 | 0.4 | 0.32692308 | Missense_variant | Variant of unknown significance |
| CRC2 | KMT2C | c.2578C>T | p.Pro860Ser | 0.28372093 | 0.37468983 | 0.30088496 | Missense_variant | Variant of unknown significance |
| CRC2 | KMT2C | c.2726G>A | p.Arg909Lys | 0.11396011 | 0.08239095 | 0.08474576 | Missense_variant | Variant of unknown significance |
| CRC2 | KMT2C | c.2917A>G | p.Arg973Gly | 0.17253521 | 0.18382353 | 0.19023136 | Missense_variant | Variant of unknown significance |
| CRC2 | KMT2C | c.2961C>G | p.Tyr987X | 0.13969336 | 0.15479116 | 0.18092105 | stop_gained | Pathogenic |
| CRC2 | KMT2C | c.2963G>T | p.Cys988Phe | 0.50549451 | 0.50466045 | 0.55033557 | Missense_variant | Variant of unknown significance |
| CRC2 | KMT2C | c.871C>T | p.Leu291Phe | 0.62731482 | 0.69318182 | 0.73941368 | Missense_variant | Variant of unknown significance |
| CRC2 | KMT2C | c.946A>T | p.Thr316Ser | 0.80469245 | 0.73571139 | 0.81997534 | Missense_variant | Variant of unknown significance |
| CRC2 | ZFHX3 | c.2330T>C | p.Val777Ala | 0.98522168 | 0.99175824 | 1 | Missense_variant | Benign |
| | Gene | nt_change | aa_change | af_Primitive | af_Metastasis | af_Stem_cells | Effect | Impact |
| CRC3 | KMT2C | c.2573G>T | p.Trp858Leu | 0.4 | 0.15503876 | 0.20571429 | Missense_variant | Variant of unknown significance |
| CRC3 | KMT2C | c.2578C>T | p.Pro860Ser | 0.4 | 0.14482759 | 0.19148936 | Missense_variant | Variant of unknown significance |
| CRC3 | KMT2C | c.2726G>A | p.Arg909Lys | 0.09569378 | 0.11029412 | 0.07017544 | Missense_variant | Variant of unknown significance |
| CRC3 | KMT2C | c.2917A>G | p.Arg973Gly | 0.29537367 | 0.09642857 | 0.09223301 | Missense_variant | Variant of unknown significance |
| CRC3 | KMT2C | c.2961C>G | p.Tyr987X | 0.22222222 | 0.0945055 | 0.09195402 | stop_gained | Pathogenic |
| CRC3 | KMT2C | c.2963G>T | p.Cys988Phe | 0.55789474 | 0.51927438 | 0.51757813 | Missense_variant | Variant of unknown significance |
| CRC3 | KMT2C | c.871C>T | p.Leu291Phe | 0.80291971 | 0.66860465 | 0.64271047 | Missense_variant | Variant of unknown significance |
| CRC3 | KMT2C | c.946A>T | p.Thr316Ser | 0.83425414 | 0.78860104 | 0.7875895 | Missense_variant | Variant of unknown significance |
| CRC3 | ZFHX3 | c.2330T>C | p.Val777Ala | 1 | 0.992 | 0.97619048 | Missense_variant | Benign |
| | Gene | nt_change | aa_change | af_Primitive | af_Metastasis | af_Stem_cells | Effect | Impact |
| CRC4 | KMT2C | c.2573G>T | p.Trp858Leu | NA | 0.32160804 | 0.32738095 | Missense_variant | Variant of unknown significance |

**Table 3.** Continued

|      | Gene  | nt_change | aa_change  | af_Primitive | af_Metastasis | af_Stem_cells | Effect          | Impact                           |
|------|-------|-----------|------------|--------------|---------------|---------------|-----------------|----------------------------------|
| CRC4 | KMT2C | c.2578C>T | p.Pro860Ser | NA          | 0.31100479    | 0.29891304    | Missense_variant | Variant of unknown significance |
| CRC4 | KMT2C | c.2726G>A | p.Arg909Lys | NA          | 0.1097561     | 0.0620155     | Missense_variant | Variant of unknown significance |
| CRC4 | KMT2C | c.2917A>G | p.Arg973Gly | NA          | 0.16361556    | 0.16994633    | Missense_variant | Variant of unknown significance |
| CRC4 | KMT2C | c.2961C>G | p.Tyr987X   | NA          | 0.16690648    | 0.17622081    | stop_gained     | Pathogenic                       |
| CRC4 | KMT2C | c.2963G>T | p.Cys988Phe | NA          | 0.35532234    | 0.34557235    | Missense_variant | Variant of unknown significance |
| CRC4 | KMT2C | c.871C>T  | p.Leu291Phe | NA          | 0.58583106    | 0.61538462    | Missense_variant | Variant of unknown significance |
| CRC4 | KMT2C | c.946A>T  | p.Thr316Ser | NA          | 0.74333333    | 0.78506787    | Missense_variant | Variant of unknown significance |
| CRC4 | ZFHX3 | c.2330T>C | p.Val777Ala | NA          | 0.97916667    | 0.99090909    | Missense_variant | Benign                           |

by comparing BM-SC-CRC with CRC primary cell lines (HT29, CL40, LS1034, and SW1463). We found that more than 6000 genes were differentially expressed between the 2 cell types (Figure 14A and B). By performing gene ontology and Kyoto Encyclopedia of Genes and Genomes (KEGG) pathway analyses, we found that these genes were mainly involved in metabolism and neurodegenerative disorders, respectively (Figure 14C and D). We also performed a gene set enrichment analysis and found a significant enrichment of invasiveness signature as previously published by Anastassiou et al[27] (Figure 14E). Finally, we highlighted a stemness signature of 43 genes, including POU5F1, NANOG, and BMP1, enriched in our BM-SC-CRC cell lines (Figure 14F, Table 5).

## Discussion

The aim of our study was to identify and characterize cells with stem-like cell properties in BMs from CRC to have a model to study this particular cancer cell subpopulation. The final goal is to identify molecular pathway and potentially druggable molecular pathways in CSC causing BM. We have been successful in establishing 4 stem cell lines from CRC patients with brain BM. To our knowledge, this is the first study that describes the presence of CSC in BM of CRC. These cells have been described in BMs from lung cancer[23] and triple negative breast cancers.[24] More recently, CTC from patients with CRC have also been described as having stem cell features.[21]

In our study we showed that our patient-derived BM-SC-CRC cells display all hallmarks of CSCs. These cells have the ability to form metaspheres, express stem-cell markers, can differentiate into more mature CRC cells, and are capable of initiating tumor growth and self-renewal in a xenograft model in vivo. In an in ovo model these stem cell lines have invasive and migratory capabilities but also promote neo-angiogenesis. Using extreme limiting dilution analysis, the stem cell frequency was estimated between 2.8% and 6.9%. This rate is highly variable in organoid models of primary or mCRC, ranging from 0.04% to 1.8%.[28] Another study

describing CTC in metastatic CRC found this rate to be less than 5%.[21] Finally, the rate is higher in our patient-derived cell line model that is enriched in CSCs. Several stem cell markers such as CD44v6, CD44, EpCAM, Lgr5, and ALDH1, previously described in many studies on CSCs, were strongly expressed in our BM-SC-CRC cell lines.[12,15,20] CTCs positive for the expression of ALDH1 considered as SC-CRCs have been associated with short progression-free survival in mCRC patients treated by first-line palliative treatment.[29] In contrast, the loss, rather than overexpression, of CD44, CD166, and EpCAM was associated to tumor progression in CRC.[30] Moreover, it was also shown that using a xenograft model, metastases from CRC are most often seeded by Lgr5 negative cells, but in the metastatic niche, cells expressing Lgr5 were found.[31] Moreover, our BM-SC-CRCs have multi-potent differentiation ability and expressed epithelial markers such as CK20 and CK19 as well as CDX2 when grown in differentiation condition. The gold standard for CSC identification is the in vivo model, and self-renewal and tumorigenicity are the 2 hallmarks that can be observed after transplantation assays including serially transplanted assay.[25] We showed that all our cell lines are able to form tumors with characteristics and phenotype identical to parental tumor and could be serially passaged, while retaining these same characteristics. Altogether, these results confirm that our patient-derived BM-SC-CRCs have stem cell properties.

Finally, we show that BM-SC-CRCs are invasive in an in ovo model. The chicken CAM assay allows rapid assessment of tumor growth and invasive and angiogenic abilities in a three-dimensional model. CAM-xenografted tumor model was also used to evaluate breast cancer stem cells, arguing it is easy to handle and accessible, and there are no ethical or regulatory constraints as a major advantage in CSC studies by contrast to in vivo model.[32] All BM-SC-CRC cell lines were considered invasive, which is comparable with established cell lines such as HCT116.[33]

Moreover, this observation was confirmed by differential transcriptome analysis because we found a strong enrichment in invasiveness signature[27] in our BM-SC-CRCs as
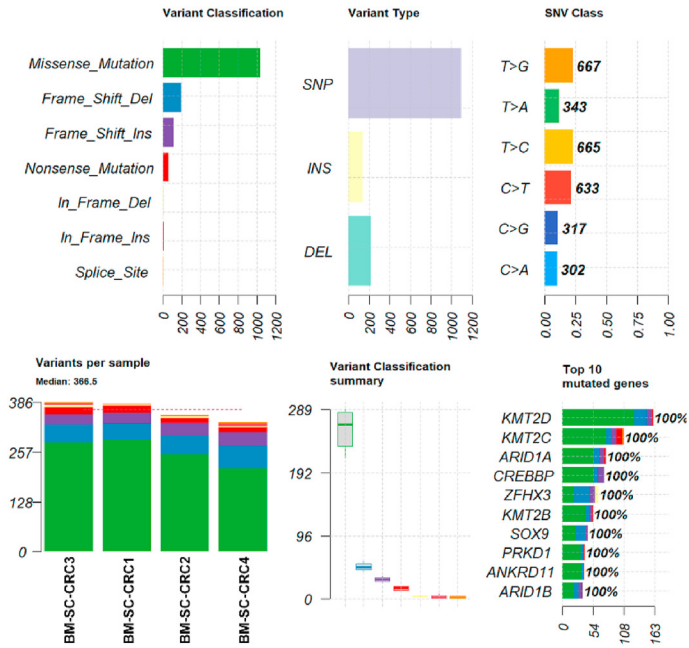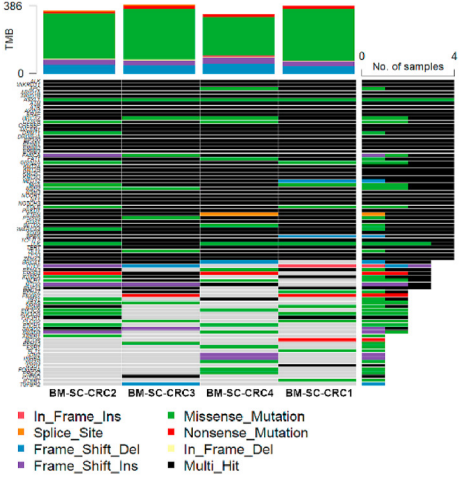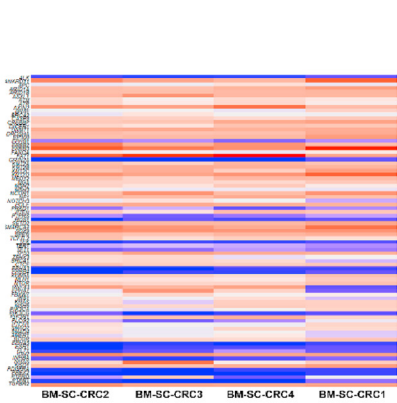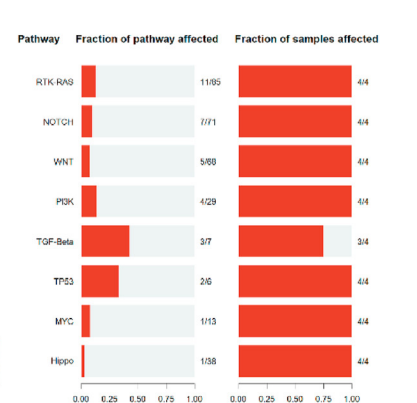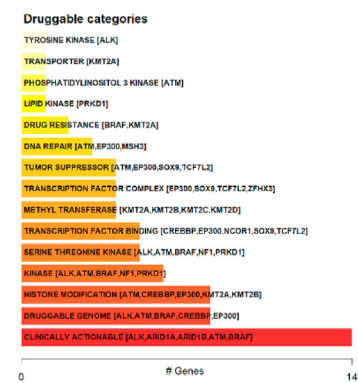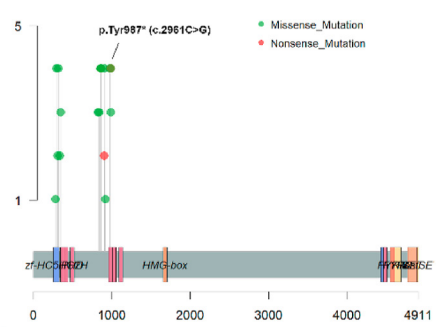
compared with cell lines from primary CRC. We also found that BM-SC-CRC lines are enriched in genes related to metabolism, oxidative phosphorylation, and ribosome, confirming previous study on circulating tumoral cells from CRC patients.[21] Nevertheless, we showed specific stemness signature enrichment, which is clearly coherent with the nature and properties of these cells. This result is also consistent with previous studies showing the impact of stemness signature in several primary tumors, including colorectal, gastric, and ovarian cancers, and its association with metastasis and prognosis.[34–36] The existence of stem cell landscape and the identification of a specific stemness signature enrichment in BM-SC-CRC could potentially be related to organ-specific colonization because it was observed in pancreatic ductal adenocarcinomas.[37] Surprisingly, we found an enrichment for several neurodegenerative disorder signatures, suggesting a neural phenotype acquisition of BM-SC-CRC.

Molecular analysis of BM-SC-CRC by whole exome sequencing showed that several mutated genes belong to the common oncogenic pathways involved in solid tumors including CRC, such as RTK-RAS, PI3K, Notch, Wnt, and SHh. Three of the 4 lines are *RAS* mutated, and all have an MSS phenotype. *RAS* mutations are found in approximately 50% of mCRC.[38–40] A higher rate of *RAS* mutation was found in mCRC with BM in a recent series but also identified that BMs (85%) were more frequently mutated than the paired primary tumor (62%).[6]

To finish, the analysis of primary tumors, BMs, and their derived cancer stem cell lines led to the identification of several *KMT2C* mutations that are common in all patients and conserved along tumor progression. KMT2C, also known as MLL3, is involved in maintenance of histone 3 lysine 4 monomethylation (H3K4me1) levels at enhancer elements and consequently regulates genes expression.[41] *KMT2C* is frequently mutated in cancer and particularly altered in breast, lung, prostate, and colon adenocarcinoma.[42] Moreover, somatic mutations in *KMT2C* have been identified as potential drivers of tumorigenesis in multiple tumors.[43] Mutations of KMT2C were found in 25% of lung cancer samples; however, the mutation frequency in BM was up to 50%, indicating the positive selection of KMT2C mutations during metastasis.[44] Several studies have also showed the impact of *KMT2C* mutations in carcinoma progression notably by the induction of hybrid EMT cells and enhanced metastatic capacity.[45] In breast cancer patients, *KMT2C* somatic mutation and low expression of KMT2C were independently correlated with poor overall survival and disease-free survival, respectively.[46] Another study

showed that *KMT2C* mutations were associated with a worse overall survival in CRC patients, particularly in patients with stage II or III.[47] Although the exact mechanism by which *KMT2C* mutations may promote CRC initiation or progression is still not fully understood, several studies have suggested that its mutations could affect the expression of genes involved in cell proliferation, cell cycle regulation, and DNA repair. To date, *KMT2C* is considered as tumor suppressor, and its inactivation may promote CRC development through transcriptional dysregulation of several signaling pathways with known relevance in cancer progression.[48] In the opposite, its restoration was sufficient to reduce CRC cell growth and to reinforce genome-wide H3K4me1 deposition at enhancers.[48] In regard to our results, we found that the pathogenic *KMT2C* c.2961C>G mutation identified in the 4 BM-SC-CRC cell lines generates a truncated form of this tumor suppressor protein with a loss of function. It is very interesting to note that this mutation was conserved from primary tumor to BM with stable allele frequency in all patients, questioning the fact that this specific mutation in CRC cells may contribute to the formation of distant metastasis. Recently, *KMT2C* loss of function mutations is positively correlated with immune invasion in tumoral microenvironment and could be considered as a potential predictive biomarker for immune checkpoint inhibitor use in patients.[49,50] *KMT2C* mutations may be considered in general as new potential biomarkers to identify high-risk CRC patients who may benefit from more aggressive treatments. Although our work needs more investigations, with a strong extension of patient analysis with or without BM, it opens the way to study brain metastatic CRC-specific mutations and signaling.

To conclude, we isolated and characterized for the first time stem cells from BMs of patients with CRC, but further investigations are needed to characterize these cells and understand the mechanism of brain dissemination. We must dissect the role of *KMT2C* mutation impacts and targeting to better understand CRC stem cells dissemination particularly to the brain.

# Materials and Methods
## Patient Sample Collection and Cell Culture

Colon cancer derived BM samples (n = 4) were obtained from patients with colon cancer with BM undergoing surgical tumor resection at the neurosurgery department of Poitiers University hospital. Written consent from these patients was obtained before surgical resection, and protocol has been approved by the local ethics committee (DC-

---

**Figure 13. (*See previous page*). Whole exome sequencing (WES) analysis of BM-SC-CRC.** (*A*) Summary of WES analysis from 89 genes highlighting variant classification and type, SNV class, and top 10 mutated genes. (*B*) Oncoplot of subsetted genes in the 4 BM-SC-CRC cell lines. (*C*) Heatmap of the corresponding gene expression in (*B*) in the 4 BM-SC-CRC cell lines. (*D*) Bar plot showing the enrichment of known oncogenic signaling pathways among the altered genes. (*E*) Bar plot showing potential druggable gene categories along with up to top 5 genes involved in them. (*F*) Lollipop plot of amino acid changes in the KMT2C protein. The mutation p.Tyr987* in the zinc finger domain (*magenta bars*) predicted to be pathogenic and common to the 4 BM-SC-CRC are indicated on the graph. DEL, deletion; INS, insertion; SNP, single nucleotide polymorphism; SNV, single nucleotide variant; TMB, tumor mutational burden.

**Table 4.** List of Mutated Genes Clinically Actionable

| Gene | Gene_long_name | Category_sources | Category |
|------|----------------|------------------|----------|
| ALK | ALK RECEPTOR TYROSINE KINASE | CarisMolecularIntelligence, MskImpact, FoundationOneGenes | Clinically actionable |
| ALK | ALK RECEPTOR TYROSINE KINASE | GuideToPharmacologyGenes, dGene, GO | Tyrosine kinase |
| ALK | ALK RECEPTOR TYROSINE KINASE | GuideToPharmacologyGenes, HopkinsGroom, GO | Kinase |
| ALK | ALK RECEPTOR TYROSINE KINASE | HopkinsGroom, dGene, HingoraniCasas, RussLampel | Druggable genome |
| ALK | ALK RECEPTOR TYROSINE KINASE | GO | Serine threonine kinase |
| KMT2D | LYSINE METHYLTRANSFERASE 2D | MskImpact | Clinically actionable |
| KMT2D | LYSINE METHYLTRANSFERASE 2D | GO | Histone modification |
| KMT2D | LYSINE METHYLTRANSFERASE 2D | BaderLabGenes, GuideToPharmacologyGenes | Methyl transferase |
| KMT2C | LYSINE METHYLTRANSFERASE 2C | GuideToPharmacologyGenes, BaderLabGenes | Methyl transferase |
| KMT2C | LYSINE METHYLTRANSFERASE 2C | GO | Histone modification |
| KMT2C | LYSINE METHYLTRANSFERASE 2C | MskImpact | Clinically actionable |
| TCF7L2 | TRANSCRIPTION FACTOR 7 LIKE 2 | GO | Tumor suppressor |
| TCF7L2 | TRANSCRIPTION FACTOR 7 LIKE 2 | GO | Transcription factor complex |
| TCF7L2 | TRANSCRIPTION FACTOR 7 LIKE 2 | GO | Transcription factor binding |
| NOTCH3 | NOTCH 3 | MskImpact | Clinically actionable |
| NOTCH3 | NOTCH 3 | HingoraniCasas | Druggable genome |
| EP300 | E1A BINDING PROTEIN P300 | GO | Histone modification |
| EP300 | E1A BINDING PROTEIN P300 | GO | Transcription factor binding |
| EP300 | E1A BINDING PROTEIN P300 | GO | DNA repair |
| EP300 | E1A BINDING PROTEIN P300 | GO | Transcription factor complex |
| EP300 | E1A BINDING PROTEIN P300 | GO | Tumor suppressor |
| EP300 | E1A BINDING PROTEIN P300 | MskImpact, FoundationOneGenes | Clinically actionable |
| EP300 | E1A BINDING PROTEIN P300 | HingoraniCasas | Druggable genome |
| NCOR1 | NUCLEAR RECEPTOR COREPRESSOR 1 | MskImpact | Clinically actionable |
| NCOR1 | NUCLEAR RECEPTOR COREPRESSOR 1 | GO | Transcription factor binding |
| BRAF | B-RAF PROTO-ONCOGENE, SERINE/THREONINE KINASE | dGene, GuideToPharmacologyGenes, GO | Serine threonine kinase |
| BRAF | B-RAF PROTO-ONCOGENE, SERINE/THREONINE KINASE | dGene, HopkinsGroom, RussLampel, HingoraniCasas | Druggable genome |
| BRAF | B-RAF PROTO-ONCOGENE, SERINE/THREONINE KINASE | HopkinsGroom, GuideToPharmacologyGenes, GO | Kinase |
| BRAF | B-RAF PROTO-ONCOGENE, SERINE/THREONINE KINASE | MskImpact, FoundationOneGenes, CarisMolecularIntelligence | Clinically actionable |
| BRAF | B-RAF PROTO-ONCOGENE, SERINE/THREONINE KINASE | GO | Drug resistance |
| SOX9 | SRY-BOX 9 | GO | Transcription factor complex |
| SOX9 | SRY-BOX 9 | GO | Kinase |
| SOX9 | SRY-BOX 9 | GO | Tumor suppressor |
| SOX9 | SRY-BOX 9 | GO | Transcription factor binding |
| SOX9 | SRY-BOX 9 | MskImpact | Clinically actionable |
| MSH3 | MUTS HOMOLOG 3 | GO | DNA repair |
| ARID1A | AT-RICH INTERACTION DOMAIN 1A | FoundationOneGenes, MskImpact | Clinically actionable |
| KMT2A | LYSINE METHYLTRANSFERASE 2A | BaderLabGenes, GuideToPharmacologyGenes | Methyl transferase |
| KMT2A | LYSINE METHYLTRANSFERASE 2A | GO | Drug resistance |

**Table 4.** Continued

| Gene | Gene_long_name | Category_sources | Category |
|---|---|---|---|
| KMT2A | LYSINE METHYLTRANSFERASE 2A | GO | Histone modification |
| KMT2A | LYSINE METHYLTRANSFERASE 2A | GO | Transporter |
| KMT2A | LYSINE METHYLTRANSFERASE 2A | FoundationOneGenes, MskImpact | Clinically actionable |
| KMT2A | LYSINE METHYLTRANSFERASE 2A | HingoraniCasas | Druggable genome |
| ZFHX3 | ZINC FINGER HOMEOBOX 3 | GO | Transcription factor complex |
| ATM | ATM SERINE/THREONINE KINASE | HopkinsGroom, GuideToPharmacologyGenes | Phosphatidylinositol 3 kinase |
| ATM | ATM SERINE/THREONINE KINASE | HopkinsGroom, HingoraniCasas, dGene, RussLampel | Druggable genome |
| ATM | ATM SERINE/THREONINE KINASE | CarisMolecularIntelligence, MskImpact, FoundationOneGenes | Clinically actionable |
| ATM | ATM SERINE/THREONINE KINASE | GuideToPharmacologyGenes, GO | Kinase |
| ATM | ATM SERINE/THREONINE KINASE | GuideToPharmacologyGenes, GO, dGene | Serine threonine kinase |
| ATM | ATM SERINE/THREONINE KINASE | GO | Tumor suppressor |
| ATM | ATM SERINE/THREONINE KINASE | GO | Histone modification |
| ATM | ATM SERINE/THREONINE KINASE | GO | DNA repair |
| KMT2B | LYSINE METHYLTRANSFERASE 2B | GuideToPharmacologyGenes, BaderLabGenes | Methyl transferase |
| KMT2B | LYSINE METHYLTRANSFERASE 2B | GO | Histone modification |
| NF1 | NEUROFIBROMIN 1 | GO | Serine threonine kinase |
| NF1 | NEUROFIBROMIN 1 | GO | Kinase |
| NF1 | NEUROFIBROMIN 1 | MskImpact, FoundationOneGenes | Clinically actionable |
| PRKD1 | PROTEIN KINASE D1 | GO, HopkinsGroom, GuideToPharmacologyGenes | Kinase |
| PRKD1 | PROTEIN KINASE D1 | GO | Histone modification |
| PRKD1 | PROTEIN KINASE D1 | GO | Lipid kinase |
| PRKD1 | PROTEIN KINASE D1 | GO, dGene, GuideToPharmacologyGenes | Serine threonine kinase |
| PRKD1 | PROTEIN KINASE D1 | RussLampel, dGene, HopkinsGroom, HingoraniCasas | Druggable genome |
| ARID1B | AT-RICH INTERACTION DOMAIN 1B | MskImpact | Clinically actionable |
| CREBBP | CREB BINDING PROTEIN | HingoraniCasas | Druggable genome |
| CREBBP | CREB BINDING PROTEIN | GO | Transcription factor binding |
| CREBBP | CREB BINDING PROTEIN | GO | Histone modification |
| CREBBP | CREB BINDING PROTEIN | FoundationOneGenes, MskImpact | Clinically actionable |

2018-3222, Comité Protection des Personnes CPP Ouest II). The study was performed according to the principles of the Declaration of Helsinki. Protocol was approved by the French Ministry of Higher Education, Research and Innovation (no. 2018081416455954).

Specimens were obtained within 30 minutes of the end of BM surgical resection procedure. Upon collection, tumors were mechanically dissociated and maintained in a serum-free medium (DMEM/F12; Thermo Fisher, Villebon-sur-Yvette, France) containing 20 ng/mL of bFGF (Thermo Fisher), 20 ng/mL of EGF (Thermo Fisher), N2 and B27 supplements (Gibco). Culture medium was replaced twice a week, and when metaspheres (and/or partly adherent cells) became numerous or confluent, they were enzymatically dissociated with Accutase (Merck-Millipore, St-Quentin-en-Yveline, France) into single cells, and their capacity to generate secondary and tertiary spheres was tested. The new term *metasphere* results from the contraction of metastasis and sphere in reference to gliomasphere, mammosphere, or colonosphere in which the organ of origin was used as prefix. To assess the capacity of the cells to differentiate, cells were grown in a medium containing DMEM/F12 enriched with glucose (17.5 mmol/L; Gibco), 10% FBS (Thermo Fisher) without any growth factor. Cultures were maintained at 37°C with a humidified atmosphere of 5% $CO_2$. After 4 passages, we considered that the BM-SC-CRC cell line was established.

## Clonogenic Assay in Methylcellulose

To evaluate established BM-SC-CRC cell lines self-renewal, cells were enzymatically dissociated with Accutase, and they
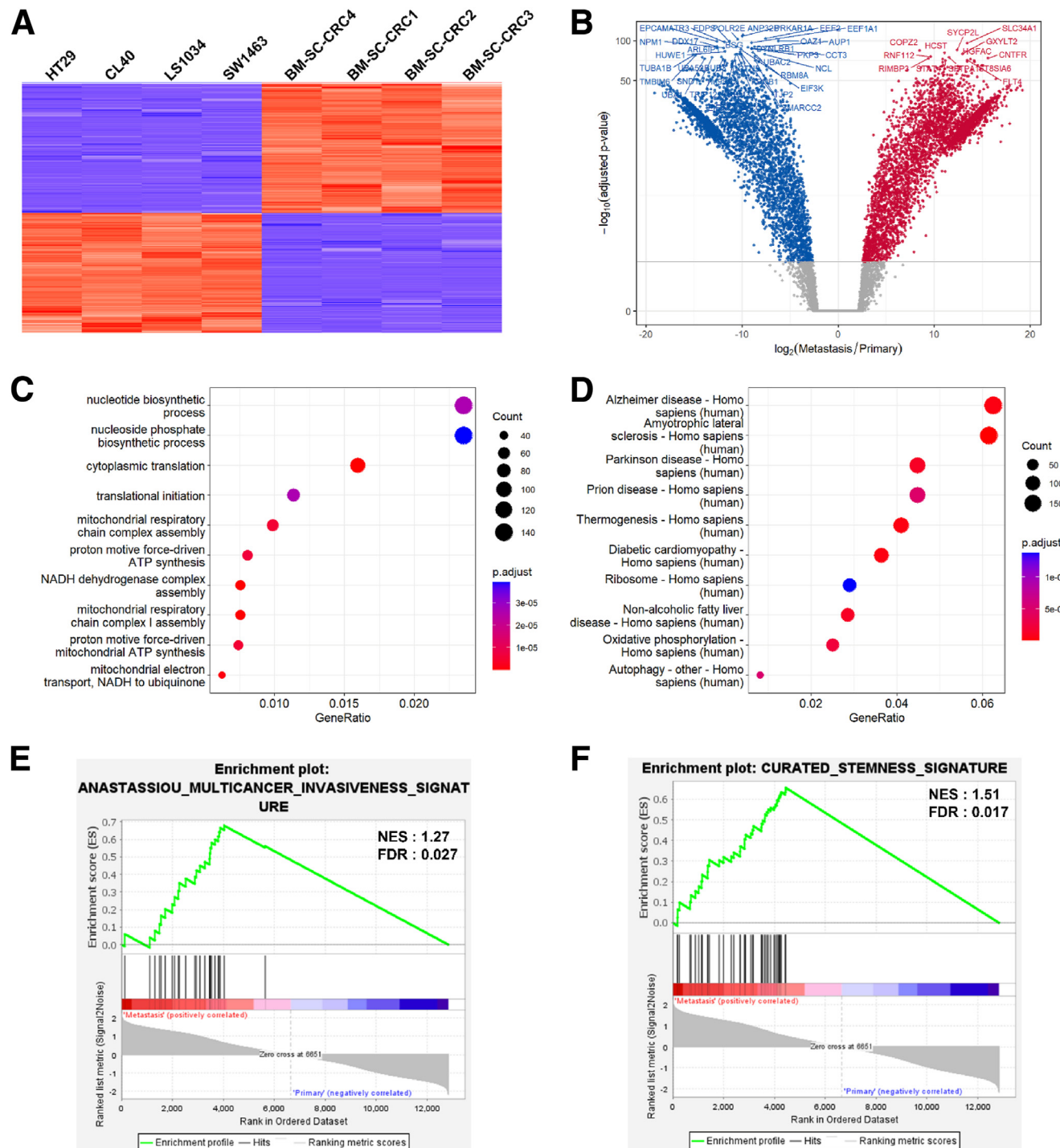
**Figure 14. Transcriptome analysis of BM-SC-CRC.** (*A*) Heatmap of differentially expressed genes between BM-SC-CRC and CRC cell lines. (*B*) Volcano plot of underexpressed (*blue*) and overexpressed (*red*) genes between BM-SC-CRC and CRC cell lines. (*C* and *D*) Dot plot of significant biological processes (c) and KEGG pathways (*D*) affected between BM-SC-CRC and CRC cell lines. (*E* and *F*) Gene set enrichment analysis showing the enrichment of invasive signature from Anastassiou (*E*) and curated stemness signature (*F*). FDR, false discovery rate; NES, normalized enrichment score.

were then plated in 30-mm culture dishes in methylcellulose medium (StemCell Technologies, Saint-Egrève, France) containing bFGF, EGF, N2 and B27 supplements. Forty thousand isolated cells were seeded per dish. After 14 days of incubation at 37°C with a humidified atmosphere of 5% $CO_2$, colonies composed of more than 50 cells were counted. The plating efficiency was then obtained with the number of colonies divided by the number of cells plated.

**Table 5.** List of Specific Stemness Genes of BM-SC-CRC

| |
|---|
| ZFP42 |
| B4GALNT1 |
| MAL |
| POU5F1 |
| LILRB4 |
| GHR |
| NCAM1 |
| GAS2 |
| LY86 |
| FHL1 |
| KANK3 |
| PGLYRP1 |
| EFHD1 |
| RNF227 |
| KRT14 |
| NANOG |
| PDGFRA |
| SLC11A1 |
| MTERF3 |
| HDC |
| SOCS2 |
| LAT2 |
| RFLNB |
| PTPRC |
| GCAT |
| WDR55 |
| PEX7 |
| LSM2 |
| BMP1 |
| RAB18 |
| GAB1 |
| ABCG2 |
| FKBP11 |
| RNF138 |
| RGS14 |
| PKD2 |
| SIRPA |
| CTSS |
| BLZF1 |
| PRPSAP1 |
| PPIC |
| TXNDC9 |
| COPRS |

## Limiting Dilutions and Metasphere-Initiating Cells Assays

To determine presence and frequency of sphere-forming cells, limiting dilution assays were performed. Metaspheres were dissociated using Accutase to obtain single-cell population. Cells were plated at limiting dilution (30 to 1 cells per well) in a 96-well plate. Half of the amount of medium was changed twice a week until day 21. The number of wells without any sphere or semi-adherent cell was calculated, and the fraction of negative wells as compared with the number of cells per well (cell dilution) was graphed to estimate metasphere-initiating cells frequency. The number of cells necessary for the formation of one sphere was then determined as described by Tropepe et al.[51] According to a Poisson distribution model, 37% (fraction at 0.37) of negative wells correspond to the dilution at which it is expected to have one metasphere-initiating cell (one sphere).

## Confocal Immunofluorescence

Metaspheres (or partly adherent cells) were plated on thin glass slides in a basal membrane matrix, Corning Matrigel (VWR, Rosny-sous-bois, France) and then fixed in 4% paraformaldehyde in phosphate-buffered saline (PBS). After washing with PBS, slides were incubated in a permeabilization/saturation solution (0.2% Triton X-100/bovine serum albumin 4%) for 1 hour at room temperature. Then, cells were incubated with primary antibodies overnight at 4°C.

## Western Blot

Proteins were subjected to electrophoretic separation using 10% polyacrylamide-sodium dodecylsulfate gel and transferred to nitrocellulose membrane (Bio-Rad System). Membranes were blocked in 1 mol/L Tris-buffer saline solution (pH 8.0) containing Tween 20 (0.1%) and non-fat dry milk (5%) for 3 hours at room temperature. Blots were then incubated overnight at 4°C with antibodies described in Materials and Methods section. Antigens were detected using horseradish peroxidase–conjugated antibody (1:1000; Cell Signaling) and an enhanced chemiluminescence kit (Bio-Rad).

## In Ovo Evaluation of Tumorigenicity and Phenotype

Fertilized White Leghorn eggs were incubated at 37.5°C with 50% relative humidity for 9 days. The CAM was dropped down by drilling a hole through the eggshell. Because some death may occur during hours after the tumor graft (an invasive surgical act), data may be collected with less than 20 eggs per group (minimum of 15 eggs per group in absence of toxicity of treatment). Total number of $3.10^6$ cells were grafted onto the CAM of each egg (n = 25). The upper portion of the CAM was removed at day 18, washed with PBS, and then transferred in PFA for 48-hour fixation. Tumor was then carefully separated from CAM tissue. Quantitative evaluation of tumor growth was then obtained by weighing. A 1 cm$^2$ portion of the lower CAM (with tumor) is collected to evaluate the number of metastatic tumor cells in 8 samples per group. Genomic DNA was extracted from these tumor cells and analyzed by quantitative polymerase chain reaction with specific primers for Human Alu sequences. Calculation of Cq for each sample, mean Cq, and relative amounts of metastases for each group were obtained and analyzed with the Bio-Rad CFX Maestro software. On day 16, a picture of the upper CAM (with tumor) was taken for quantitative evaluation of neoangiogenesis (vessels were counted by 2 different experimenters, n = 6 for control, n = 11 for BM-SC-CRC1 and n = 10 for BM-SC-CRC2).

## In Vivo Evaluation of Tumorigenicity by Orthotopic Injection

The protocol was approved by the French Ministry of National Education, Higher Education and Research (no. 2018081416455954), and all animal experimental procedures were performed in accordance with the recommendations of the European Union (2010/63/EU) for care and use of laboratory animals and conformed to the ethical guidelines of the French Ministry of Agriculture and Food (Animal Health and Protection Veterinary Service).

BALB/c nude female 8-week-old mice were used. Standardized diet (Dieta Standard 4RF21, Mucedola, Italy) and bedding (poplar litter) were used according to the recommendations of the European Union (2010/63/EU). Nesting materials were also available in ventilated cages. To establish intracranial tumor in mice the BM-SC-CRC were suspended at $10^5$ cells/$\mu$L in PBS and kept in ice until injected. Adult mice were anesthetized by xylazine/ketamine intravenous injection, and a 1-cm midline scalp incision and hole in the skull were made. One $\mu$L of $10^5$/$\mu$L tumor cell suspension was injected using a Hamilton syringe with a 27-gauge needle in the striatum (2 mm left and 2.5 mm depth of the bregma).[52,53] The skin was closed with skin clips.

Body weights were measured daily to check whether mice were healthy after surgery. After 10% loss of body weight in 24 hours, mice were killed by PFA (4%) intracardiac perfusion.

For serial injection, mice were killed by gas euthanasia with $CO_2$ gradient. Tumors were recovered after death (between 3 and 12 weeks according to patient cell line aggressiveness), and cells were seeded in basal conditions during approximately 2 weeks. Cells ($10^5$ cells/$\mu$L in PBS) were injected in a second mouse to allow tumor development (same experiment as described above). Brains were harvested, and pathologic analysis with H&E staining and CDX2/CK20 staining was performed by a pathologist from Pathology Department of Poitiers University hospital.

Data concerning antibodies, clonogenic assay in methylcellulose, in ovo assay, whole exome sequencing, RNA sequencing, microsatellite instability analysis, and statistical analysis are provided in the Materials and Methods section.

## Whole Exome Sequencing

DNA was extracted from paraffin-embedded tissue (CRC or BM of patients) with a tumor cellularity greater than 30%. Six $\times$ 10 $\mu$m formalin-fixed paraffin-embedded sections were subject to a deparaffinization protocol using Tween 20 detergent before DNA extraction with the Maxwell 16 FFPE Tissue LEV Purification kit. DNA was quantified by Quantus Fluorometer (Promega, Madison, WI). Genomic DNA from cell lines was extracted using the Maxwell 16 LEV DNA Purification kit (Promega). Library preparation was performed by using the SureSelectXTHS Enzymatic Fragmentation Kit and SureSelectXTHS Human All Exon V7 Target Enrichment System (Agilent, Santa Clara, CA), according to the manufacturer's instructions. Library sequencing was performed by using a NextSeq 550 system (Illumina, San Diego, CA) high output run using v2 chemistry. Paired-end reads of 150 base pair lengths were generated in accordance with the supplied protocol. Samples were sequenced to median average depth of 150$\times$ (PRJNA1014113; https://www.ncbi.nlm.nih.gov/sra).

Data were converted to FastQ format using bcl2fastq2-v2.20.0.422 (Illumina, San Diego, CA). Reads were aligned to GRCh37 (hg19) using bwa-0.7.17 (Li H and Durbin R, 2009; PMID: 19451168). Alignments were sorted, and duplicates were marked by using picard-2.18.2 (Picard Toolkit, 2019; Broad Institute, GitHub Repository, http://broadinstitute.github.io/picard/), variant calling was performed by using a custom-made variant caller GRVC (Gustave Roussy Variant Caller), and coverage statistics were compiled by using picard-2.18.2. Targeted regions were considered sufficiently covered if the median depth of coverage across all samples was $\geq$20$\times$ at target positions. Variants were annotated with snpEff-v4.3.[54] Annotated VCF files were converted to MAF files by using vcf2maf tools. Then, MAF files were subsetted for a panel of 89 genes selected from TCGA and MSKCC studies available at cBio-Portal (https://www.cbioportal.org) by presenting a mutation rate more than 3% in CRC. Among these genes, we selected variants with a quality phred of more than 30, read depth (dp)of more than 100, and exclude variants located in 5′ and 3′ untranslated region as well as synonym variants. Finally, these subsetted maf files were analyzed with maftools[55] under R environment to get number and types of variants and to generate oncoplot and drug-gene interactions.

## RNA Sequencing

The RNAs were extracted by using the RNeasy Mini Kit (Qiagen) following the manufacturer's protocol and qualified using the Agilent 2100 Bioanalyzer platform (Agilent Technologies). Qualified RNAs were sent to the MGX platform in Montpellier for RNA sequencing. Briefly, libraries were produced by using a TruSeq Stranded mRNA Sample Preparation Kit (Illumina) and 150nt paired-end sequenced on NovaSeq sequencer (Illumina). The fastq files were deposited in the Sequence Read Archive database (https://www.ncbi.nlm.nih.gov/sra) under the accession number (PRJNA1013918). Raw data were processed using STAR and featureCounts as mapping and counting tools, respectively. Differential expression analysis was performed by using the DESeq2 R package. The R package ComplexHeatmap and clusterProfiler were used to generate heatmap and gene ontology analysis, respectively. Gene set enrichment analysis was performed using GSEA tool from Broad Institute (http://www.gsea-msigdb.org/gsea/login.jsp). We curated 43 genes from 4 different stemness gene sets[56–59] to get a significant and specific stemness signature of our BM-SC-CRC.

## Microsatellite Instability Analysis

The microsatellite instability/stability status was analyzed by using the MSI Analysis kit (Promega) and the geneMapper software (Applied). Analyzed microsatellites

are the pentaplex panel of quasi-monomorphic mono-nucleotides markers (NR21, BAT25, BAT26, NR24, and Mono27).

## Antibodies

The primary antibodies used in our assays were directed against CD133 (polyclonal, Cell Signaling, 1:250), CD44 (monoclonal, Cell Signaling, 1:250), CD44v6 (monoclonal, R&D Systems, 1:250), CK20 (monoclonal, Sigma, 1:500), EpCAM (monoclonal, Cell Signaling, 1:250), ALDH1 (polyclonal, Cell Signaling, 1:250), CK19 (monoclonal, Abcam, 1:250), CDX-2 (polyclonal, Abcam, 1:250), and actin (1:5000, Cell Signaling). Alexa Fluor 488-, 555- or 647-conjugated antibodies (1:250, Invitrogen) and/or tetramethylrhodamine-phalloidin (1:50) and/or DAPI (4′,6-diamidino-2-phenylindole, Life Technologies) were used as secondary antibodies and nuclear marker. Coverslips were mounted with Mowiol (Calbiochem, Darmstadt, Germany) before observation with confocal microscopy (FV1000, Olympus).

## Statistical Analysis

Descriptive statistics of the results were calculated with GraphPad Prism 6 (GraphPad Software, La Jolla, CA). All experiments were performed at least 3 times. Statistical significance was evaluated by two-way analysis of variance (WB) and Grubb's tests (in ovo) (*$P < .05$, **$P < .01$, ***$P < .001$).

## References

1. Berghoff AS, Schur S, Fureder LM, et al. Descriptive statistical analysis of a real life cohort of 2419 patients with brain metastases of solid cancers. ESMO Open 2016;1:e000024.
2. Cagney DN, Martin AM, Catalano PJ, et al. Incidence and prognosis of patients with brain metastases at diagnosis of systemic malignancy: a population-based study. Neuro Oncol 2017;19:1511.
3. Roussille P, Auvray M, Vansteene D, et al. Prognostic factors of colorectal cancer patients with brain metastases. Radiother Oncol 2021;158:67.
4. Mege D, Sans A, Ouaissi M, et al. Brain metastases from colorectal cancer: characteristics and management. ANZ J Surg 2018;88:140.
5. Muller S, Kohler F, Hendricks A, et al. Brain metastases from colorectal cancer: a systematic review of the literature and meta-analysis to establish a guideline for daily treatment. Cancers (Basel) 2021;13.
6. Roussille P, Tachon G, Villalva C, et al. Pathological and molecular characteristics of colorectal cancer with brain metastases. Cancers (Basel) 2018;10.
7. Brastianos PK, Carter SL, Santagata S, et al. Genomic characterization of brain metastases reveals branched evolution and potential therapeutic targets. Cancer Discov 2015;5:1164.
8. Croker AK, Allan AL. Cancer stem cells: implications for the progression and treatment of metastatic disease. J Cell Mol Med 2008;12:374.
9. Al-Hajj M, Wicha MS, Benito-Hernandez A, et al. Prospective identification of tumorigenic breast cancer cells. Proc Natl Acad Sci U S A 2003;100:3983.
10. Hervieu CN, Battu S, Mathonnet M. The role of cancer stem cells in colorectal cancer: from the basics to novel clinical trials. Cancers (Basel) 2021;13:1092.
11. Singh SK, Hawkins C, Clarke ID, et al. Identification of human brain tumour initiating cells. Nature 2004;432:396.
12. Dalerba P, Dylla SJ, Park IK, et al. Phenotypic characterization of human colorectal cancer stem cells. Proc Natl Acad Sci U S A 2007;104:10158.
13. Ricci-Vitiani L, Lombardi DG, Pilozzi E, et al. Identification and expansion of human colon-cancer-initiating cells. Nature 2007;445:111.
14. Creighton CJ, Li X, Landis M, et al. Residual breast cancers after conventional therapy display mesenchymal as well as tumor-initiating features. Proc Natl Acad Sci U S A 2009;106:13820.
15. O'Brien CA, Pollett A, Gallinger S, et al. A human colon cancer cell capable of initiating tumour growth in immunodeficient mice. Nature 2007;445:106.
16. Huang EH, Hynes MJ, Zhang T, et al. Aldehyde dehydrogenase 1 is a marker for normal and malignant human colonic stem cells (SC) and tracks SC overpopulation during colon tumorigenesis. Cancer Res 2009;69:3382.
17. Kemper K, Prasetyanti PR, De Lau W, et al. Monoclonal antibodies against Lgr5 identify human colorectal cancer stem cells. Stem Cells 2012;30:2378.
18. Leng Z, Xia Q, Chen J, et al. Lgr5+CD44+EpCAM+ strictly defines cancer stem cells in human colorectal cancer. Cell Physiol Biochem 2018;46:860.
19. Pang R, Law WL, Chu AC, et al. A subpopulation of CD26+ cancer stem cells with metastatic capacity in human colorectal cancer. Cell Stem Cell 2010;6:603.
20. Todaro M, Gaggianesi M, Catalano V, et al. CD44v6 is a marker of constitutive and reprogrammed cancer stem cells driving colon cancer metastasis. Cell Stem Cell 2014;14:342.
21. Grillet F, Bayet E, Villeronce O, et al. Circulating tumour cells from patients with colorectal cancer have cancer stem cell hallmarks in ex vivo culture. Gut 2017;66:1802.
22. de Souza Neto FP, Bernardes SS, Marinello PC, et al. Metformin: oxidative and proliferative parameters in-vitro and in-vivo models of murine melanoma. Melanoma Res 2017;27:536.
23. Nolte SM, Venugopal C, McFarlane N, et al. A cancer stem cell model for studying brain metastases from primary lung cancer. J Natl Cancer Inst 2013;105:551.
24. McGowan PM, Simedrea C, Ribot EJ, et al. Notch1 inhibition alters the CD44hi/CD24lo population and reduces the formation of brain metastases from breast cancer. Mol Cancer Res 2011;9:834.
25. Clarke MF, Dick JE, Dirks PB, et al. Cancer stem cells: perspectives on current status and future directions—AACR workshop on cancer stem cells. Cancer Res 2006;66:9339.
26. Tang DG. Understanding cancer stem cell heterogeneity and plasticity. Cell Research 2012;22:457.
27. Anastassiou D, Rumjantseva V, Cheng W, et al. Human cancer cells express Slug-based epithelial-mesenchymal transition gene expression signature obtained in vivo. BMC Cancer 2011;11:529.

28. Regan JL, Schumacher D, Staudte S, et al. Non-canonical hedgehog signaling is a positive regulator of the WNT pathway and is required for the survival of colon cancer stem cells. Cell Rep 2017;21:2813.

29. Gazzaniga P, Gradilone A, Petracca A, et al. Molecular markers in circulating tumour cells from metastatic colorectal cancer patients. J Cell Mol Med 2010;14:2073.

30. Lugli A, Iezzi G, Hostettler I, et al. Prognostic impact of the expression of putative cancer stem cell markers CD133, CD166, CD44s, EpCAM, and ALDH1 in colorectal cancer. Br J Cancer 2010;103:382.

31. Fumagalli A, Oost KC, Kester L, et al. Plasticity of Lgr5-negative cancer cells drives metastasis in colorectal cancer. Cell Stem Cell 2020;26:569.

32. Pinto MT, Ribeiro AS, Conde I, et al. The chick chorioallantoic membrane model: a new in vivo tool to evaluate breast cancer stem cell activity. Int J Mol Sci 2020:22.

33. Brattain MG, Fine WD, Khaled FM, et al. Heterogeneity of malignant cells from a human colonic carcinoma. Cancer Res 1981;41:1751.

34. Chen X, Zhang D, Jiang F, et al. Prognostic prediction using a stemness index-related signature in a cohort of gastric cancer. Frontiers in Molecular Biosciences 2020; 7:570702.

35. Wang W, Guo H, Wu S, et al. Construction of metastasis-specific regulation network in ovarian cancer based on prognostic stemness-related signatures. Reproductive Sciences 2023.

36. Wei R, Quan J, Li S, et al. Integrative analysis of biomarkers through machine learning identifies stemness features in colorectal cancer. Frontiers in Cell and Developmental Biology 2021;9:724860.

37. Zheng H, Liu H, Li H, et al. Characterization of stem cell landscape and identification of stemness-relevant prognostic gene signature to aid immunotherapy in colorectal cancer. Stem Cell Research & Therapy 2022;13:244.

38. Van Cutsem E, Kohne CH, Hitre E, et al. Cetuximab and chemotherapy as initial treatment for metastatic colorectal cancer. N Engl J Med 2009;360:1408.

39. Venook AP, Niedzwiecki D, Lenz HJ, et al. Effect of first-line chemotherapy combined with cetuximab or bevacizumab on overall survival in patients with KRAS wild-type advanced or metastatic colorectal cancer: a randomized clinical trial. JAMA 2017;317:2392.

40. Vincenzi B, Cremolini C, Sartore-Bianchi A, et al. Prognostic significance of K-Ras mutation rate in metastatic colorectal cancer patients. Oncotarget 2015;6:31604.

41. Sze CC, Shilatifard A. MLL3/MLL4/COMPASS family on epigenetic regulation of enhancer function and cancer. Cold Spring Harb Perspect Med 2016;6.

42. Kandoth C, McLellan MD, Vandin F, et al. Mutational landscape and significance across 12 major cancer types. Nature 2013;502:333.

43. Sjoblom T, Jones S, Wood LD, et al. The consensus coding sequences of human breast and colorectal cancers. Science 2006;314:268.

44. Liu Z, Zheng M, Lei B, et al. Whole-exome sequencing identifies somatic mutations associated with lung cancer metastasis to the brain. Annals of Translational Medicine 2021;9:694.

45. Cui S, Chen Y, Guo Y, et al. Hsa-miR-22-3p inhibits liver cancer cell EMT and cell migration/ invasion by indirectly regulating SPRY2. PloS One 2023;18:e0281536.

46. Liu X, Qiu R, Xu M, et al. KMT2C is a potential biomarker of prognosis and chemotherapy sensitivity in breast cancer. Breast Cancer Research and Treatment 2021;189:347.

47. Cho SJ, Yoon C, Lee JH, et al. KMT2C mutations in diffuse-type gastric adenocarcinoma promote epithelial-to-mesenchymal transition. Clinical Cancer Research 2018;24:6556.

48. Larsson C, Cordeddu L, Siggens L, et al. Restoration of KMT2C/MLL3 in human colorectal cancer cells reinforces genome-wide H3K4me1 profiles and influences cell growth and gene expression. Clin Epigenetics 2020; 12:74.

49. Liu D, Benzaquen J, Morris LGT, et al. Mutations in KMT2C, BCOR and KDM5C predict response to immune checkpoint blockade therapy in non-small cell lung cancer. Cancers (Basel) 2022;14.

50. Liu R, Niu Y, Liu C, et al. Association of KMT2C/D loss-of-function variants with response to immune checkpoint blockades in colorectal cancer. Cancer Science 2023.

51. Tropepe V, Sibilia M, Ciruna BG, et al. Distinct neural stem cells proliferate in response to EGF and FGF in the developing mouse telencephalon. Dev Biol 1999; 208:166.

52. Gaillard A, Decressac M, Frappe I, et al. Anatomical and functional reconstruction of the nigrostriatal pathway by intranigral transplants. Neurobiol Dis 2009;35:477.

53. Gaillard A, Prestoz L, Dumartin B, et al. Reestablishment of damaged adult motor pathways by grafted embryonic cortical neurons. Nat Neurosci 2007;10:1294.

54. Cingolani P, Platts A, Wang le L, et al. A program for annotating and predicting the effects of single nucleotide polymorphisms, SnpEff: SNPs in the genome of Drosophila melanogaster strain w1118; iso-2; iso-3. Fly (Austin) 2012;6:80.

55. Mayakonda A, Lin DC, Assenov Y, et al. Maftools: efficient and comprehensive analysis of somatic variants in cancer. Genome Res 2018;28:1747.

56. Malta TM, Sokolov A, Gentles AJ, et al. Machine learning identifies stemness features associated with oncogenic dedifferentiation. Cell 2018;173:338.

57. Patel AP, Tirosh I, Trombetta JJ, et al. Single-cell RNA-seq highlights intratumoral heterogeneity in primary glioblastoma. Science 2014;344:1396.

58. Ramalho-Santos M, Yoon S, Matsuzaki Y, et al. "Stemness": transcriptional profiling of embryonic and adult stem cells. Science 2002;298:597.

59. Venteicher AS, Tirosh I, Hebert C, et al. Decoupling genetics, lineages, and microenvironment in IDH-mutant gliomas by single-cell RNA-seq. Science 2017;355.

**Correspondence**
Address correspondence to: Amandine Desette, PhD, Prodicet LAB-UR24144-PBS-Batiment B37-1, rue Georges Bonnet-86073, Poitiers, France. e-mail: amandine.desette@univ-poitiers.fr, amandine.desette@chu-poitiers.fr.

## CRediT Authorship Contributions

Amandine Desette, PhD (Conceptualization: Lead; Data curation: Equal; Formal analysis: Equal; Investigation: Equal; Methodology: Equal; Software: Equal; Writing – original draft: Lead; Writing – review & editing: Equal)

Pierre-Olivier Guichet, PhD (Conceptualization: Equal; Data curation: Equal; Formal analysis: Equal; Methodology: Equal; Software: Lead; Validation: Equal; Writing – review & editing: Equal)

Sheik Emambux, MD (Conceptualization: Supporting; Formal analysis: Supporting; Writing – original draft: Equal; Writing – review & editing: Supporting)

Konstantin Masliantsev, PhD (Conceptualization: Equal; Data curation: Equal; Formal analysis: Equal; Methodology: Equal; Validation: Supporting; Writing – review & editing: Equal)

Ulrich Cortes, PhD (Data curation: Equal; Formal analysis: Equal; Methodology: Supporting; Writing – review & editing: Supporting)

Birama Ndiaye, PhD (Data curation: Equal; Formal analysis: Supporting; Methodology: Supporting; Writing – review & editing: Supporting)

Serge Milin, MD (Data curation: Supporting; Formal analysis: Equal; Methodology: Equal; Writing – review & editing: Supporting)

Simon George, PhD (Formal analysis: Equal; Methodology: Supporting)

Mathieu Faigner, MD (Data curation: Supporting; Formal analysis: Supporting; Writing – review & editing: Supporting)

Julie Tisserand, MD (Data curation: Supporting; Formal analysis: Supporting; Writing – review & editing: Supporting)

Afsaneh Gaillard, PhD (Data curation: Equal; Methodology: Equal; Writing – review & editing: Supporting)

Sébastien Brot, PhD (Data curation: Equal; Methodology: Supporting; Writing – review & editing: Supporting)

Michel Wager, MD, PhD (Data curation: Equal; Methodology: Supporting; Writing – review & editing: Supporting)

David Tougeron, MD, PhD (Conceptualization: Equal; Funding acquisition: Lead; Project administration: Lead; Resources: Lead; Supervision: Equal; Validation: Supporting; Writing – review & editing: Equal)

Lucie Karayan-Tapon, MD, PhD (Conceptualization: Lead; Funding acquisition: Lead; Methodology: Lead; Resources: Lead; Supervision: Lead; Validation: Equal; Writing – review & editing: Equal)

## Conflicts of interest

The authors disclose no conflicts.